Article:
Todd, MC, Allen, CJT, Bart, M et al. (25 more authors) (2013) Meteorological and dust aerosol conditions over the western Saharan region observed at Fennec Supersite-2 during the intensive observation period in June 2011. Journal of Geophysical Research D: Atmospheres, 118 (15). 8426 - 8447. ISSN 0148-0227

https://doi.org/10.1002/jgrd.50470

Meteorological and dust aerosol conditions over the western Saharan region observed at Fennec Supersite-2 during the intensive observation period in June 2011

M. C. Todd,[1,2] C. J. T Allen,[3] M. Bart,[4] M. Bechir,[5] J. Bentefouet,[6] B. J. Brooks,[7] C. Cavazos-Guerra,[1] T. Clovis,[6] S. Deyane,[5] M. Dieh,[5] S. Engelstaedter,[3] C. Flamant,[8] L. Garcia-Carreras,[4] A. Gandega,[5] M. Gascoyne,[4] M. Hobby,[4] C. Kocha,[8] C. Lavaysse,[8] J. H. Marsham,[4,7] J. V. Martins,[9] J. B. McQuaid,[4] J. B. Ngamini,[10] D. J. Parker,[4] T. Podvin,[11] A. Rocha-Lima,[9] S. Traore,[5] Y. Wang,[1] and R. Washington[3]

Received 23 October 2012; revised 2 May 2013; accepted 4 May 2013; published 15 August 2013.

[1] The climate of the Sahara is relatively poorly observed and understood, leading to errors in forecast model simulations. We describe observations from the Fennec Supersite-2 (SS2) at Zouerate, Mauritania during the June 2011 Fennec Intensive Observation Period. These provide an improved basis for understanding and evaluating processes, models, and remote sensing. Conditions during June 2011 show a marked distinction between: (i) a "Maritime phase" during the early part of the month when the western sector of the Sahara experienced cool northwesterly maritime flow throughout the lower troposphere with shallow daytime boundary layers, very little dust uplift/transport or cloud cover. (ii) A subsequent "heat low" phase which coincided with a marked and rapid westward shift in the Saharan heat low towards its mid-summer climatological position and advection of a deep hot, dusty air layer from the central Sahara (the "Saharan residual layer"). This transition affected the entire western-central Sahara. Dust advected over SS2 was primarily from episodic low-level jet (LLJ)-generated emission in the northeasterly flow around surface troughs. Unlike Fennec SS1, SS2 does not often experience cold pools from moist convection and associated dust emissions. The diurnal evolution at SS2 is strongly influenced by the Atlantic inflow (AI), a northwesterly flow of shallow, cool and moist air propagating overnight from coastal West Africa to reach SS2 in the early hours. The AI cools and moistens the western Saharan and weakens the nocturnal LLJ, limiting its dust-raising potential. We quantify the ventilation and moistening of the western flank of the Sahara by (i) the large-scale flow and (ii) the regular nocturnal AI and LLJ mesoscale processes.

Citation: Todd, M. C., et al. (2013), Meteorological and dust aerosol conditions over the western Saharan region observed at Fennec Supersite-2 during the intensive observation period in June 2011, *J. Geophys. Res. Atmos.*, *118*, 8426–8447, doi:10.1002/jgrd.50470.

1. Introduction

1.1. The Nature of the Saharan Climate System

[2] The atmospheric boundary layer over the Sahara (SABL) is a unique and important feature of the global climate system, exhibiting numerous extremes. During boreal summer, in particular, intense surface heating produces the deepest boundary layers on Earth of up to 6 km [*Cuesta et al.*, 2009], and the associated development of the Saharan heat low (SHL), over a huge, largely uninhabited expanse of northern Mali, southern Algeria, and Mauritania (Figure 1). The SHL is a result of the development of a likely dome-shaped thermal heating feature in the lower troposphere below ~700 hpa and is essentially the summertime position of the wider West African heat low (WAHL). The SHL plays a pivotal role in the West African Monsoon

This article is a companion to *Marsham et al.* [2013] doi:10.1002/jgrd.50211.

[1]University of Sussex, UK.
[2]Now at Aeroqual Limited, Auckland, New Zealand.
[3]University of Oxford, UK.
[4]School of Earth and Environment, University of Leeds, UK.
[5]Office National de Météorologie, Mauritanie.
[6]AeroEquip & Conseil, Douala, Cameroon.
[7]National Center for Atmospheric Science, University of Leeds, UK.
[8]Laboratoire Atmosphères, Milieux, Observations Spatiales, CNRS and Université Pierre et Marie Curie, Paris, France.
[9]University of Maryland, Baltimore County (UMBC), USA.
[10]ASECNA, Dakar-Yoff, Senegal.
[11]LOA, University of Lille, France.

Corresponding author: M. C. Todd, University of Sussex, UK. (m.todd@sussex.ac.uk)

2169-897X/13/10.1002/jgrd.50470

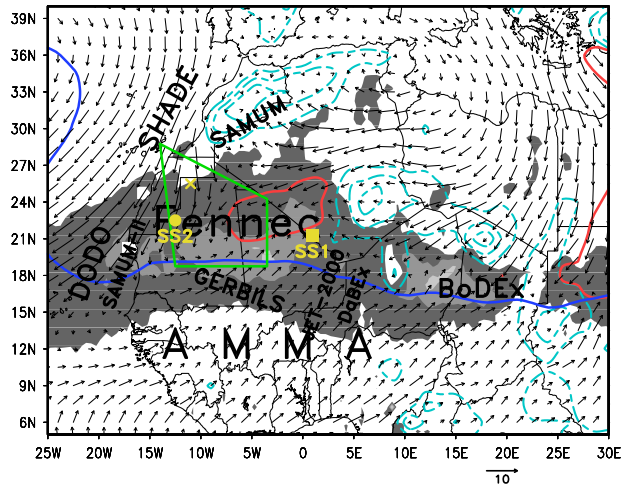

Figure 1. The Fennec domain and climatology. Figure shows mean (2000–2012) June–Sept. aerosol optical depth (AOD) from satellite MISR data (shaded, contour intervals are 0.4, 0.6, and 0.8) and key mean June–September circulation features derived from ERA-Interim reanalysis data (1979–2012), specifically the mean 925 hPa winds (arrows); the mean position of the Saharan heat low core (1008 hPa contour of sea level pressure, thick red contour); the mean position of the inter-tropical discontinuity (solid blue line, as defined by the 10 gkg^{-1} contour of 925 hPa specific humidity). Figure also highlights the location of the two supersites (SS1 yellow square, SS2 yellow circle), the Bir Moghrein sampling station (yellow cross) and approximate aircraft flight zone (green polygon). Also indicated are surface elevation (dashed cyan contour, 1000, 1500, and 2000 m) and the approximate location of recent field campaigns.

[e.g., *Sultan et al*., 2003]. Further, this region is also where the highest vertically integrated dust aerosol loading anywhere in the Earth's atmosphere is found. Several satellite-derived aerosol products show that the SHL is co-located with the aerosol maximum during the boreal summer [*Engelstaedter et al*., 2006] (Figure 1). Saharan dust aerosols have a complex interaction with the regional and global climate through: (i) The direct effect of dust aerosols on the shortwave and longwave radiative flux, which can exceed many tens Wm^{-2} at the TOA and in excess of 100 WM^{-2} at the surface [*Haywood and Boucher*, 2000]. (ii) The indirect effect of dust aerosols on cloud microphysical processes and properties [e.g., *Kaufman et al*., 2005]. (iii) The semi-direct effect of dust generated by absorptional heating within dust layers, which changes relative humidity and vertical stability [*Dunion and Velden*, 2004]. (iv) Atmospheric chemical processes on aerosol surfaces [*Cwiertny et al*., 2008]. (v) The influence of Saharan dust deposition on terrestrial and marine bio-geochemical cycles [e.g., *Jickells et al*., 2005; *Mahowald et al*., 2010]. A wide range of meteorological dust generation mechanisms is responsible for this aerosol "hotspot" over the SHL region (see *Knippertz and Todd* [2012] for a review).

[3] However, the central Sahara, with no significant population centers, suffers from a particularly sparse observational network, which hinders our understanding of the climate, with profound consequences for weather forecasting and climate prediction in the region and beyond. It should be noted that the SHL characteristics as described by reanalyses data like those in Figure 1 may be subject to considerable uncertainty given the lack of data for assimilation into the model. *Haywood et al*. [2005] and *Milton et al*. [2008] showed large biases due to dust processes in Numerical Weather Prediction model outgoing longwave radiation (of ~50 Wm^{-2}) and surface net radiation (of ~100 Wm^{-2}), respectively. Such errors in radiation lead to errors in key dynamical features beyond the Sahara (e.g., the African Easterly Jet), with consequences for tropical cyclone development in the Atlantic and the circulation over the Mediterranean basin. It has been shown that including effects of dust aerosols into numerical models has a beneficial impact on weather and climate simulations [*Perez et al*., 2006; *Rodwell and Jung*, 2008; *Tompkins et al*., 2005].

1.2. The Project "Fennec: The Saharan Climate System"

[4] In the last decade or so, a number of field campaigns have been undertaken to improve our baseline data on meteorological and aerosol conditions in the wider North African sector (Figure 1). These include Jet2000 [*Thorncroft et al*., 2003], SHADE in 2001 [*Haywood et al*., 2003], the Bodélé Dust Experiment (BoDEx) in 2005 [*Todd et al*., 2007; *Washington et al*., 2006], the African Monsoon Multidisciplinary Analysis (AMMA) in 2006 [*Redelsperger et al*., 2006], the Dust and Biomass Experiment DABEX in 2006 [*Haywood et al*., 2008], Dust Outflow and Deposition to the Ocean in 2006 [*McConnell et al*., 2008], the Geostationary Earth Radiation Budget Intercomparison of Long-wave and Short-wave radiation in 2007 [*Haywood et al*., 2011], and the Saharan Mineral Dust Experiment in 2006 and 2008 [*Ansmann et al*., 2011]. With the exception of limited measurements during AMMA [*Cuesta et al*. 2008; *Messager et al*., 2010], no previous campaign has focused on the SHL region of North Africa during the summer dust season (Figure 1).

[5] Fennec is an international consortium with research groups in the UK, France, Germany, and the USA working in collaboration with the Meteorological Services of Algeria, Mauritania in North Africa, and the European partner countries. Fennec was conceived and designed to fill critical gaps in observations and understanding of the Saharan climate system including the role of mineral dust aerosol. To this end, Fennec involved a large-scale, multi-platform, surface, and airborne observational campaign in the SHL region over an extended period during 2011–2012 to quantify the physical processes controlling the Saharan climate system. These unique observations are then used in combination with operational and research-oriented numerical models to analyze aerosol, radiative, land surface, thermodynamic, and dynamic processes over the Sahara to evaluate and attribute errors in weather and climate models for this region.

[6] The ground-based field campaign is a cornerstone of Fennec and has three components: high temporal resolution, multi-parameter observations of the atmosphere at two main supersites, with SS1 in Southern Algeria and Supersite-2 (SS2) in Northern Mauritania (Figure 1), and less comprehensive observations of surface meteorology from a network of remote automatic stations distributed across the SHL region [*Hobby et al*., 2012]. The SSs are strategically located as close as possible to the heart of the SHL/aerosol maximum as logistics allowed. SS2 is located to the west of the mean SHL and aerosol maximum and as such is indicative of

Table 1. Instruments Deployed at SS2 During Fennec IOP 2011

Instrument	Deployment	Sampling Frequency	Manufacturer	Notes
Radiosonde	1–30 June	Three times daily at 00:00, 06:00, and 12:00 UTC	Vaisala RS92 GPS	No data on: 1 and 3; 06 and 12 UTC on 2 and 4; 06 UTC on 13; 00 UTC on 24. 5 June 18 UTC only. 25–30 additional data at 09 UTC.
Sodar (1650–2750 Hz)	1–30 June	10 min	Scintec	Problems with overheating through the IOP
Pilot balloons (PIBAL)	11–30 June	Twice daily at 09.00 and 17:00 UTC		
Flux tower	1–30 June	10 min (from 10 Hz data)	University of Leeds; Metek USA-1 sonic anemometers; E-pulse ee04 humidity sensor, Hukseflux ground heat-flux sensor; Kipp & Zonen CNR4 radiometers	Substantial data loss after 20 June
Sun photometer	1–30 June	15 min	Cimel C-138	
LACO Aerosol Sampling Station – (LASS)	23 May–26 June	Average 6 hourly	Laboratory for Aerosol, Clouds, and Optics (LACO) at the University of Maryland, Baltimore County (UMBC)	

conditions over the broad western Saharan region. This paper, and the companion paper for SS1 by *Marsham et al.* [2012], aims to provide an overview of the surface observations during Fennec. Here, we focus specifically on the observational program at the Fennec SS2. We present analysis of results from the ground-based instruments, contextualized with analyses from Fennec research aircraft observations, reanalysis, satellite sources, and numerical models where appropriate. Section 2 describes the instrument characteristics. Section 3 presents our results, in which we focus on the synoptic-seasonal-scale evolution of the atmospheric structure over western Saharan region (section 3.1) and SS2 (section 3.2), a focus on two specific components of the lower-level circulation, namely the Atlantic inflow (AI) (section 3.3) and the low-level jet (LLJ) (section 3.4) which play important roles in the heat and moisture budgets of the western Saharan region and proximate SHL. We then consider dust aerosol conditions at SS2 in this context (section 3.5) before summarizing the mean diurnal cycle (section 3.5). Discussion and conclusion are presented in section 4.

2. The Instruments Deployed at Fennec SS2 and Additional Data Used

[7] Fennec SS2 is located in northern Mauritania near the town of Zouerate at 22.75°N, 12.48°W and an elevation of 343 m above sea level (Figure 1). This location was selected as the nearest location on the western flank of the SHL/aerosol maximum with a reliable infrastructure. It is also relatively close to the Fennec aircraft campaign base at Fuerteventura in the Canary Island (Figure 1) allowing overflights to support radiation budget closure experiments. Fennec SS1, in southern Algeria is located towards the center/eastern flank of the mean SHL. The Fennec instruments at SS2 were deployed by the Office National de Météorologie (ONM) in Mauritania at the end of May 2011 in the environs of the airport at Zouerate close to the existing World Meteorological Organisation (WMO) station 61404. A suite of meteorological and aerosol instruments were deployed at SS2-Zouerate (Table 1) to measure key meteorological and aerosol quantities. The core instruments of the flux tower and Cimel sun photometer instrument were deployed for the Extended Observation period of one-year duration from June 2011 to June 2012. Additional instruments to provide greater detail on the vertical structure of the SABL were deployed for the shorter intensive observation period (IOP) from 1 to 30 June 2011. In addition, during the IOP, an aerosol sampling instrument was deployed some 290 km to the north of SS2 at the remote town of Bir Moghrein 25.23°N, 11.62°W (Figure 1). This location was selected to ensure no contamination of physical aerosol samples from the mining activities at Zouerate. Instruments were deployed and operated by the ONM Mauritanie. The characteristics of the instruments are described below.

[8] The Fennec flux tower consisted of 15 m high mast instrumented with 20 Hz sonic anemometers at 10 and 15 m. At 2 m, there were passively ventilated measurements of temperature and humidity, as well as pressure. A separate 2 m mast was used to measure upwelling and downwelling solar and longwave radiative fluxes, and ground heat flux at 10 cm. Radiosondes were launched three times daily at 00:00, 06:00, and 12:00 UTC on all days during the IOP except on 25–30, when four launches per day were made at 00:00, 06:00, 09:00, and 12:00 UTC. SS2 local time is the same as UTC. Afternoon soundings were not made, due to a limited number of trained staff, working one shift per day. Reducing sampling occurred on 26 (06:00 and 12:00 UTC only), 13 (00 and 12:00 UTC), 2 and 4 (00:00 UTC only), and 5 (18:00 UTC only). There were no observations made on 1 and 3 June 2011. To increase sampling, we make use of both the radiosonde ascent and descent profiles, which covers a period of around 90 min, although vertical resolution from the descent is reduced. We present analysis of individual ascents and of data interpolated to a grid with 20 m vertical resolution and 1-hourly temporal resolution over the period 00:00 to 14:00 UTC during which time observations were most frequent. No interpolation is made during the mid-afternoon-evening period when data are absent.

[9] Pilot balloons (hereafter "pibals") were released twice daily at 0900 and 1700 UTC and used to derive wind speed throughout their ascent, using a single theodolite method. These data complement the radiosonde and sodar wind measurements. The vertical extent of pibal wind estimates varied partly as a function of aerosol and wind conditions between

Table 2. WRF Configuration

Model Name	WRF
Reference	*Michalakes et al*. [2005]
Boundary conditions	ERA-Interim reanalyses
Domain	Inner nest: 18.5°–27°N, 20°W–8°W
Horizontal grid spacing	9 km outer domain and 3 km inner nest.
Vertical levels	60
Simulation period	10–19 June 2011
Height of lowest layer	10 m
Physical schemes	Microphysics: Lin et al. 2003 scheme PBL: Mellor-Yamada-Janjic TKE scheme (MYJ) Surface: Unified Noah land-surface model. Cumulus convection: Grell-3D

~500 m and greater than 10,000 m. Vertically integrated aerosol conditions were observed using a Cimel C-318 sun photometer, installed as part of the AErosol RObotic NETwork (AERONET) [*Holben et al*., 1998]. A Scintec MFAS phased array sodar was deployed, and the vertical profile of wind speed and direction was retrieved at a nominal 10-min temporal and 10-m vertical resolution. Although the sodar was identical to that at SS1, the sampling rate in the afternoon however was often poor due to instrument overheating. Due to these problems, the results from sodar require considerable post-processing and are not included in this paper.

[10] Some dropsonde measurements from research flights are also discussed. Flights with the French F-20 and the British BAe146 aircraft were made: the FF22 flight (F-20 aircraft) and various BAe146 flights (with labels such as B607 and B608) are used here. Both aircraft used the Vaisala RD93 sonde.

[11] In addition, in situ aerosol samples were collected at Bir Moghrein using the Laboratory for Aerosol Clouds and Optics (LACO) Aerosol Sampling Station (LASS). LASS is an automatic system for collection of aerosol particles on filters designed and built by LACO at the University of Maryland Baltimore County, USA. The station has a cartridge with eight sampling positions for Nuclepore filters (with one of the positions reserved for reference blank filters); each position is separated in two stages for the collection of fine (nominal aerodynamic diameter $d < 1.5$ μm) and coarse (1.5 μm $< d < 10$ μm) particles. The station PM10 inlet and filter cartridges were installed at a height of 3 m a.g.l. Each one of the eight sampling positions in the cartridge is connected individually through vacuum tubes to the automatic control and vacuum system at the ground level. LASS was operational from 23 May to 26 June, collecting between three and four filters daily between 07:00 and 13:00 UTC, 13:00 and 19:00 UTC, 19:00 and 21:00 UTC, and 21:00 and 07:00 UTC. The fine and coarse Nuclepore filters collected by LASS will be submitted to gravimetric analysis, elemental composition, optical reflectance techniques, and electron microscopy for determination of size distribution and shape of the particles. Preliminary samples have been analyzed for a selection of samples discussed here.

[12] The Fennec observational data set was also complemented with contextual information from (i) ERA-Interim global atmospheric reanalysis fields [*Dee et al*., 2011] produced by the European Center for Medium-Range Weather Forecasts (ECMWF). We use the high-resolution 0.5° horizontal grid and 60 model sigma-level data. (ii) The ECMWF operational analyses at 1.125° which have 91 model levels. In addition, we supplement Fennec observations with SYNOP reports from the WMO station 61640 at Zouerate reporting at 06:00, 09:00, 12:00, 15:00, and 18:00 UTC daily. A simulation using the Weather Research and Forecasting (WRF) mesoscale model was conducted for the period 11–19 June 2011 with a configuration summarized in Table 2. We also utilize information of dust aerosol distribution from the Spinning Enhanced Visible and InfraRed Imager (SEVIRI) instrument on the geostationary Meteosat Second Generation (MSG) satellites. Based on infrared channels, a false-color dust product has been developed described by *Lensky and Rosenfeld* [2008], in which dust appears in pink tones as a result of contrast between the 12.0 and 10.8 um channels and high emissivity of dust in the 8.7 um channel.

3. Results and Discussion

3.1. Synoptic Overview of the IOP at SS2

[13] Here we consider the synoptic-scale structure of the atmosphere in the North African sector during June 2011. In many key components of the large-scale circulation relevant to conditions at SS2, a distinction can be made between two periods within the IOP. These roughly correspond to an early period from 2–12 June and a latter period from 13 to the end of the month. These phases are equally pertinent to the conditions at SS1 in southern Algeria, as described in the companion paper of *Marsham et al*. [2012]. With respect to conditions at SS2, we refer to these periods as the "Maritime phase" and "heat low phase", respectively, and described in more detail in section 3.2. During the Maritime phase, the upper level pattern exhibited a trough centered over the Iberian Peninsula extending southwards over the northern extremity of North Africa, driving mid and upper level anomalous westerlies over northwest Africa and SS2 (Figure 2a). Subsequently, over the latter heat low phase of 13–25, June, anomalous positive geopotential heights dominated over Iberia and the extremity of northwest Africa, associated with the passage of three upper level ridges, driving an anomalous mid and upper level easterly flow, with absolute easterlies at lower levels, over the western Saharan sector and SS2 (Figure 2b).

[14] The summertime low-level circulation over western North Africa is dominated by the climatological features of the Azores high and the SHL. During the Maritime phase, the Azores high ridged towards the coast of northwest Africa and moved westward subsequently (not shown). The SHL has a pronounced seasonal cycle [*Lavaysse et al*., 2009] involving a southeast to northwest migration from its position to the south of the Hoggar mountains (~18°N, 5°E) in May to its most northerly position close to 24°N and 0°W during July and August. The mean date of transition between these two states is 20 June [*Lavaysse et al*., 2009]. In 2011 the transition occurred on 11 June, associated with the maritime-heat low phase transition. During early June 2011 (Figure 3a), the SHL remained relatively stationary in an anomalously eastern location (~15°E), similar to the mean state for May with strong northwesterly inflow of maritime air over much of the western Saharan region. From 13 June, the SHL exhibited an abrupt westward displacement (to ~5–10°W), with two distinct intraseasonal pulses. As

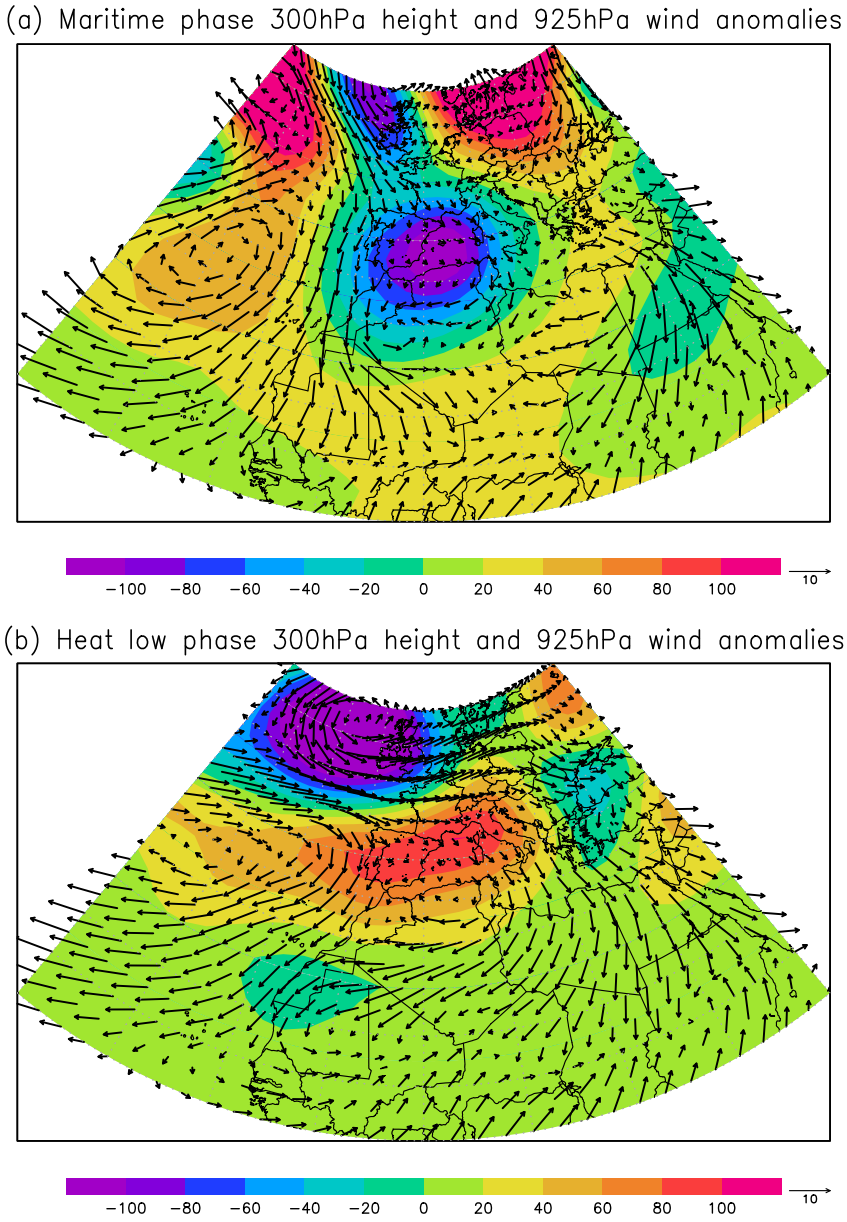

Figure 2. Circulation during the "maritime" and "heat low" phases of Fennec IOP. (a) Mean anomalies of 300 hPa geopotential height and absolute 925 hPa winds from ERA-Interim data during 1–11 June 2011. (b) As Figure 2a but for 13–25 June 2011.

such, the Maritime phase (heat low phase) experienced an eastward (westward) displaced SHL with the northwestward shift (although operating at intraseasonal timescales), occurring in the middle of June 2011, broadly consistent with the mean seasonal cycle and "transition" to the summertime state of the SHL during late June. These two phases are broadly congruent with the "east" and "west" phases of the intraseasonal heat low mode of variability described from statistical analysis of reanalysis data by *Chauvin et al.* [2010] and the conceptual modes of the AI described by *Grams et al.* [2010]. In the Maritime phase ("heat low east"), the Sahara is effectively "ventilated" by cool advection from the Atlantic sector restricting the heat low to the central/eastern Sahara. In contrast, during the heat low phase ("heat low west"), the Sahara is "ventilated" substantially by cool advection over Libya and the SHL shifts to the western Sahara. *Chauvin et al.* [2010] identify the southward penetration of Rossby wave disturbances over Europe and North Africa as the likely driver of phase shifts.

[15] The westward propagation of monsoon troughs embedded within African Easterly Waves (AEW) is known to be important for various dust emission processes [*Knippertz and Todd*, 2010]. During the Maritime phase, the AEW activity over continental North Africa was suppressed. From around 13 June onwards during the heat low phase, a sequence of westward propagating troughs is apparent (Figure 3a). As a result, the Maritime phase experienced extensive northwesterly flow across the western Saharan region sector. In contrast, the heat low phase of Fennec IOP 2011 exhibited a strong easterly and northeasterly synoptic-scale flow over central Algeria, northern Mali, and Northern Mauritania, around the northern flank of the heat low and

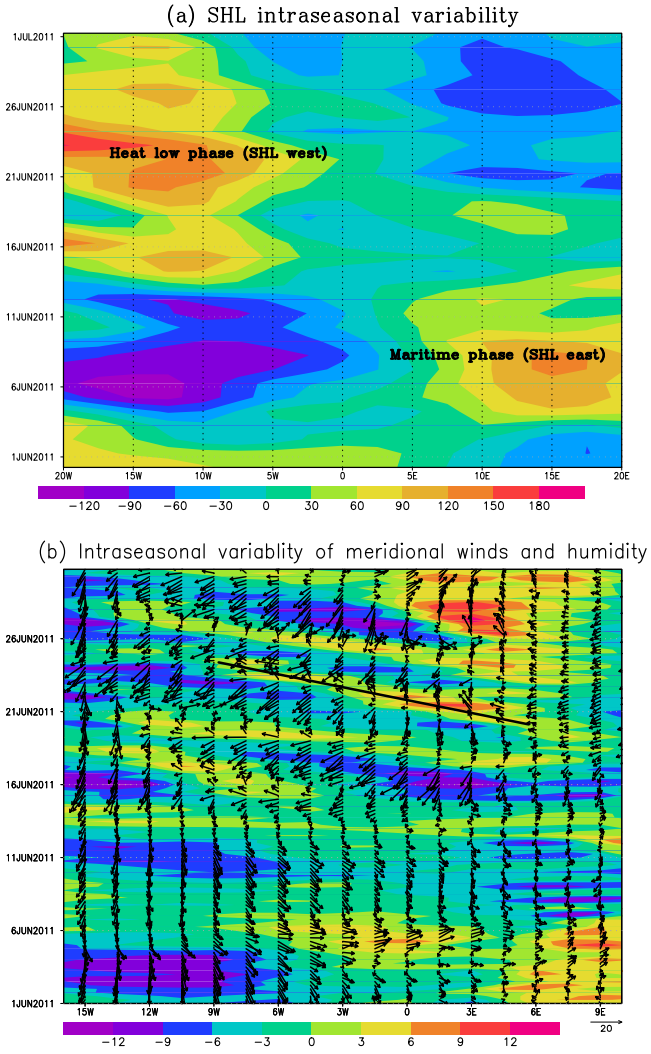

Figure 3. The low-level circulation during Fennec IOP. (a) Time-longitude plot of absolute SHL intensity anomalies (defined as the thickness of the 925–700 hPa layer from *Lavaysse et al.* [2009]) averaged between 20 and 25°N. (b) Time-longitude plot of 850 hPa meridional winds (shaded) averaged over 20–25°N, with 925 hPa specific humidity (0.01 gkg^{-1} contour) and 925 hPa winds at latitude of SS2 (22.75°N). Thick black line denotes location of example AEW trough. Note different longitudinal range in the Figures 3a and 3b.

AEW troughs (Figures 3a and 3b, respectively). These structures strongly influenced the local meteorology and aerosol conditions observed at SS2 during the Fennec IOP, as explained below.

3.2. Characteristic Atmospheric Structure at SS2 During "Maritime" and "Heat Low" Phases

[16] The influence of the large-scale circulation associated with the Maritime and heat low phases is readily apparent in the observations at SS2. Radiosondes (Figure 4a) show the Maritime phase is characterized by

[17] 1. A cool, dry lower troposphere below about 500 hPa, in which westerlies extend from the top of the convective boundary layer (CBL) throughout the troposphere, providing large-scale advective cooling of the Saharan atmosphere.

[18] 2. Development of a moist daytime CBL up to ~880 hPa at 12:00 UTC (Figure 4a red line) with a ~5°K potential temperature inversion "lid" above the CBL.

[19] 3. Relatively weak nocturnal surface temperature inversion at 00:00 UTC (Figure 4a green line) (but not evident at 06:00 UTC, yellow line in Figure 4a, as explained in section 3.4)

[20] In contrast, the heat low phase (Figure 4b) is characterized by

[21] 1. A deep, dry almost dry-adiabatic layer from the top of the CBL at ~850 hPa to the free troposphere at ~550 hPa, namely the Saharan residual layer (SRL), advected from the central Sahara (based on samples of back-trajectory analyses (not shown)). Potential temperatures at 800 hPa are ~10°K higher than during the Maritime phase.

[22] 2. Maximum relative humidity values near the top of the SRL are frequently close to values for shallow convective cloud formation.

[23] 3. A cool, moist CBL below the SRL, which develops through the day (Figure 4b red line). By the end of the month cases where an almost "pure" well-mixed SABL occur, where temperatures are near dry-adiabatic from the surface to the top of the SRL (Figure 4b red line).

[24] Both phases experience a nocturnal, shallow, mixed relatively cool, moist near surface layer, with north-northwesterly flow (evident at 06:00UTC in the yellow lines in Figures 4a and 4b), indicative of AI (see section 3.3.) and a typically northeasterly LLJ above (see section 3.4). The LLJ maximum is in the inversion capping the stable nocturnal boundary layer at 00:00 UTC or the AI at 06:00 UTC.

[25] The transition from the maritime to heat low phases over the IOP is illustrated in the time series from radiosondes (Figure 5) and surface observations (Figure 6). Profiles of potential temperature (Figure 5a) show a distinction between the cool maritime lower tropospheric conditions with little evidence of a SRL before 14 June, and the hotter well-mixed SRL, which is well developed from 20 June onwards. The strong mid-tropospheric westerlies are apparent in the Maritime phase followed by slacker easterlies (Figures 5d and 5e). The CBL at 12:00 UTC is generally slightly deeper during the heat low phase, up to ~880 hPa (Figure 4b red line) compared to the Maritime phase, up to ~850 hPa (Figure 4a red line). Typically boundary layer heights (calculated as the height at which the potential temperature is 0.5 K greater than that at 930 hPa, following *Marsham et al.* [2012]) at the time of last daily observation (~13.30TC) are quite low for the Sahara; ~1500 m in the heat low phase and about 1000 m in the Maritime phase, but in some cases towards the end of the heat low phase, the sonde descent does indicate a nearly well-mixed boundary layer up to 5000 m in height (Figure 4b red line). Clearly, however, we do not sample the full extent of afternoon boundary-layer development. Nearly well-mixed boundary layers up to ~5 km, height, respectively, are observed from dropsondes released from the Fennec research aircraft flights at locations 250 km northeast of SS2 during the mid-late afternoon periods on 21 and 22 June (Figure 4c). It is interesting to note that the contrasting conditions between the Maritime phase and heat low phase are evident in data from SS1 [*Marsham et al.*, 2012], where, despite SS1's continental location, CBL depths of ~2 km and ~5 km, respectively, were observed.

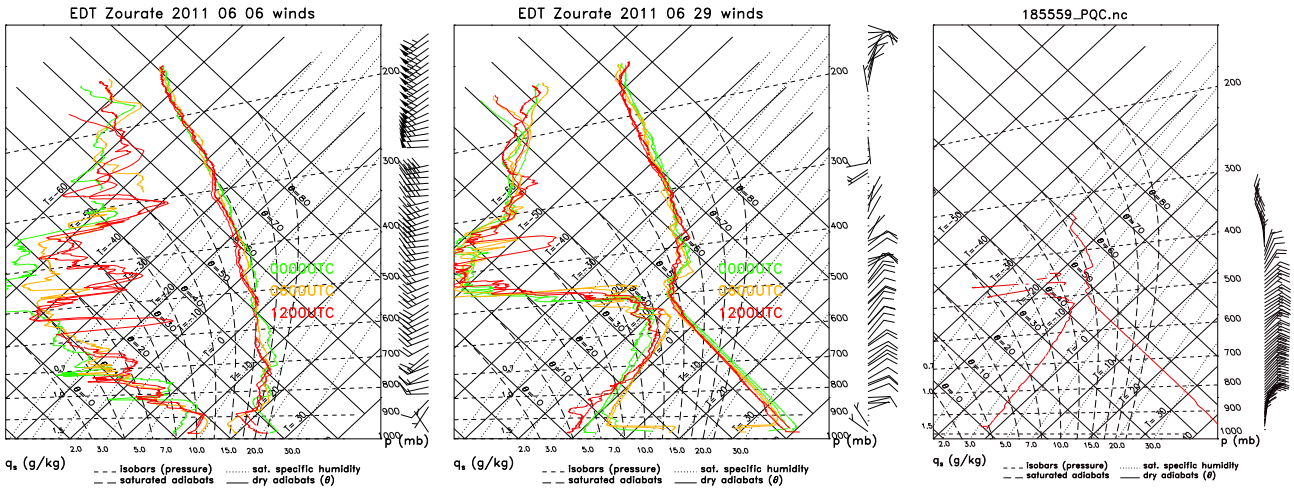

Figure 4. (a) Tephigrams from radiosondes at SS2 characteristic of (a) the IOP Maritime phase on 6 June and (b) the heat low phase on 29 June. Green, yellow, and red lines are from the 00:00, 06:00, and 12:00 UTC, respectively. Wind barbs are shown for the 06:00 UTC radiosonde only. (c) Tephigram from flight B608 dropsonde at 18:55 UTC on 22 June at 23.5°N, 9.2°W.

[26] Low-level moisture (Figure 5b, typically around 10 gkg^{-1}) is concentrated in the lowest ~700 m a.g.l. with deeper moist layers during the Maritime phase, and more variable conditions during the heat low phase, associated with periods of hot, dry advection from the central Sahara. Moisture flux (Figure 5f) is consistent over the period and is dominated by moisture flux in the LLJ and AI (see sections 3.3. and 3.4), clearly indicating the nocturnal moistening of the western Saharan sector, for even with a northeasterly LLJ, the moisture flux typically re-circulates towards the Sahara further south of SS2 (Figure 2b). Mid-tropospheric moisture (Figure 5b) is higher (>5 gkg^{-1} at 3000 m) during the heat low phase compared to the Maritime phase (<1 gkg^{-1}) indicating greater vertical mixing during the daytime of low-level moisture which was advected into the SHL during the previous night. The Maritime phase after 3 June is substantially cloud-free over SS2 (Figure 6f) and indeed much of the western Saharan sector of Mauritania, Northern Mali,

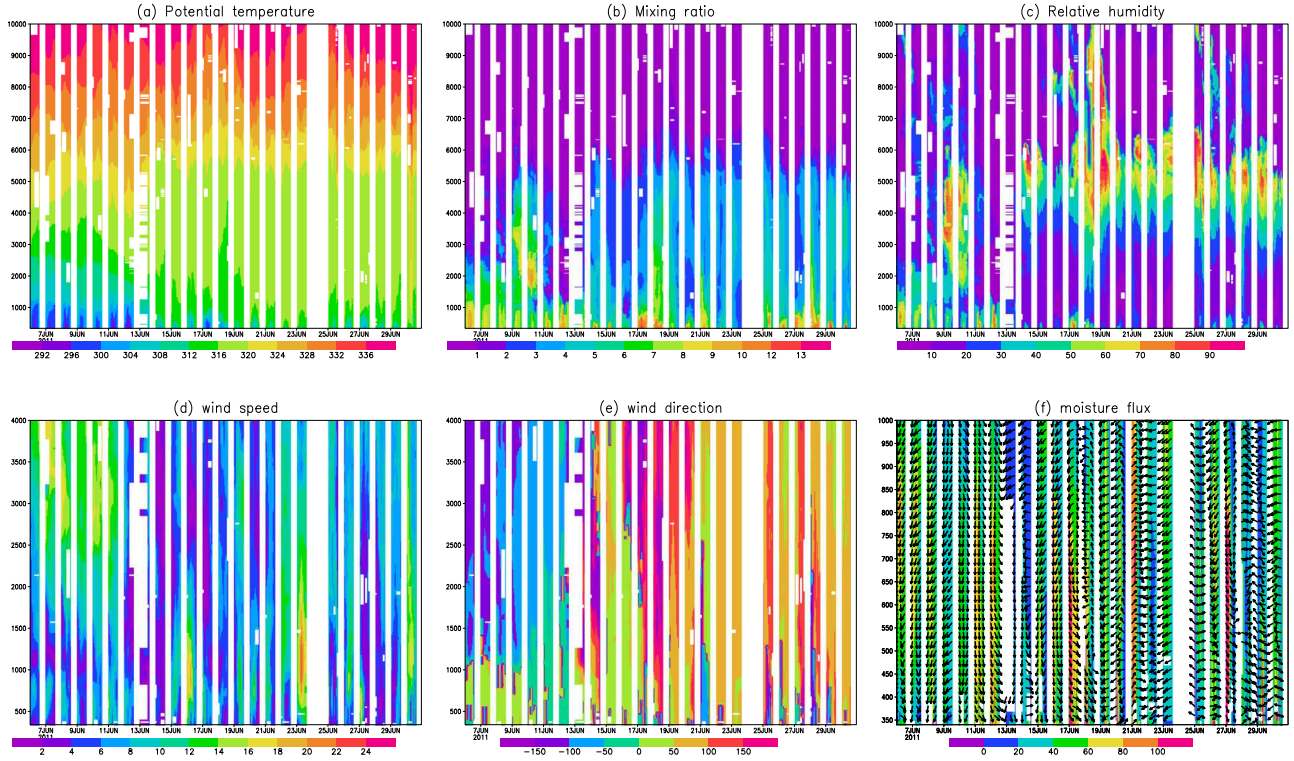

Figure 5. Time series at SS2 of the vertical profile of (a) potential temperature (K), (b) WVMR (gkg^{-1}), (c) relative humidity (%), (d) wind speed (ms^{-1}), (e) wind direction (degrees from north), and (f) WVMR flux ($gkg^{-1}\,ms^{-1}$). Note different height range in Figures 5d–f compared to Figures 5a–c.

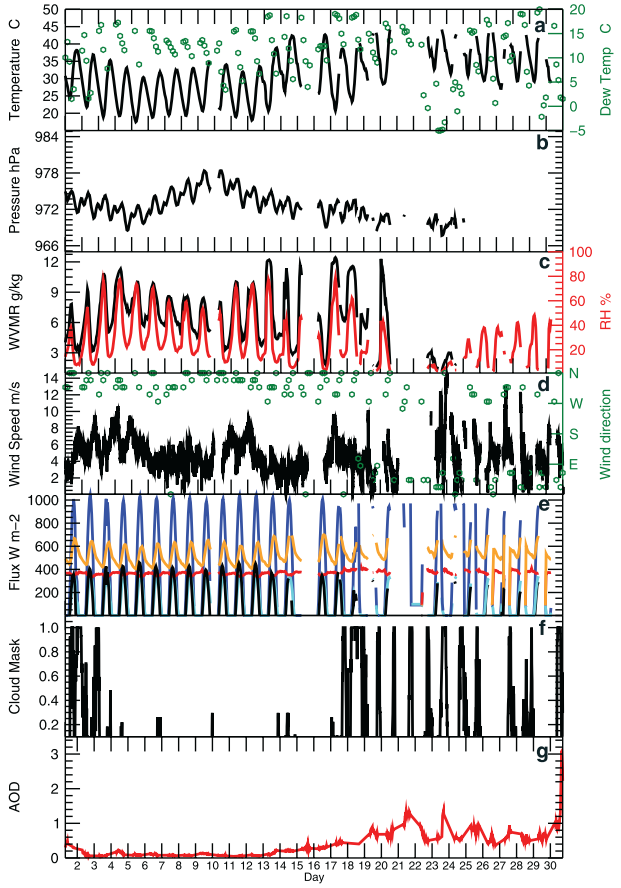

Figure 6. Time series of near surface conditions at SS2. (a) Temperature (black line) and dew point temperature (green dots) (°C). (b) Pressure (hPa). (c) Water vapor mixing ratio (black line, gkg^{-1}) and relative humidity (red line, %). (d) 10-m height wind speed from Fennec flux tower (black line, ms^{-1}) and wind direction from SYNOPS reports (green dots). (e) Radiative fluxes (WM^{-2}); SW down (blue), SW up (cyan), LW down (red), LW up (orange), net radiation (black). (f) SEVIRI cloud fraction at SS2. (g) Aeronet AOD.

and Western Algeria (Figure 7a). During the heat low phase at SS2, high relative humidity (Figure 5c) is observed at the top of the SABL close to 5000 m, sufficient for shallow convective cloud development during the evening (Figure 6f), apparent too over the wider western Saharan domain (e.g., Figure 7f). In the south of the western Saharan domain during the heat low phase, mesoscale convective system (MCS) activity is observed on some days to the south of SS2, e.g., 20 June (Figure 7d) associated with moist monsoon surges in the in AEW trough (Figure 3b). Atmospheric aerosol loadings (Figure 6g, pink coloring in Figure 7) are much higher during the heat low phase compared to the Maritime phase, as discussed in detail in section 3.5.

[27] The surface daytime maximum temperatures rise from the low 30s °C in the early phase to low 40s °C by the end of the IOP, while the minima rise from the high 10s °C to the high 20s °C (Figure 6a). Moreover, despite greater cloud cover, the magnitude of the nocturnal near-surface temperature inversions is far higher in the heat low phase (compare green/yellow lines in Figure 4b with Figure 4a) such that nocturnal decoupling of the surface from near-surface conditions is greater. Water vapor mixing ratios (WVMR) observations are sparse after the middle of the month, but SYNOP dew-point temperatures (Figure 6a) indicate pronounced variability during the heat low phase, with particularly dry conditions on 22–24 and 29–30 June when Td values <0°C are observed. Whilst SS2 lies too far north to be frequently under the influence of the monsoon flow, the passage of AEW troughs (Figure 3b) was indicated by higher WVMR on 17–18, 21, and 27–29 June (Figure 5d). The dry *Harmattan* northeasterly flow is most pronounced on 22–25 June.

3.3. AI at SS2

[28] The Sahara is bounded to the west by the relatively cool Atlantic and advection of maritime air over the western Saharan by a meso-synoptic-scale circulation; the AI (in [*Grams et al*. 2010]) is important to maintenance of heat and moisture budgets of both the West African Monsoon *Peyrille and Lafore* [2007] and the SHL [*Lavaysse et al*., 2009]. Our observations indicate that SS2 experiences the effects of the AI. During the day, the balance between horizontal advection of cool maritime air and turbulence in the CBL over land results in a stationary sea breeze front at the coast. Once turbulence dies down in the evening, the sea breeze front penetrates inland such that the AI is a nocturnal feature over coastal western Saharan [*Grams et al*., 2010]. Our model simulations (Figure 8a) show that the AI extends over the Atlantic coast of West Africa from ~15°N to ~28°N (beyond which topography prevents inland penetration) and penetrates many hundreds of km inland by 07:00 UTC the time of maximum extent, with a mean northerly component north of 20°N (and therefore at SS2) transitioning to a mean westerly component between 15 and 20°N.

[29] At SS2, the morning arrival of the AI can be identified from the 06:00 UTC radiosonde data and surface observations as a cool moist near surface layer in the early morning hours (yellow lines in Figures 4a and 4b). On the basis of the 0000 and 06:00 UTC radiosonde ascents (Figures 4a and 4b and Figure 5d), the AI is apparent on over 60% of days (on some heat low phase days, and on all days in the Maritime phase), as a shallow, cool, moist well-mixed moist layer between the surface and ~100–600 m height a.g.l with WVMR of ~8–13 gkg^{-1} and weak northwesterly winds. The mean depth of the AI layer is 158 m a.g.l., but the AI depth is quite variable (standard deviation = 150 m) with the Maritime phase exhibiting far higher values. Above this, AI layer lies in the LLJ discussed in section 3.4. The structure of the AI in the bottom few hundred meters at 06:00 UTC is clearly distinct from that at 00:00 UTC, when the development of a weak surface temperature inversion below the relatively hot and dry CBL from the preceding afternoon is evident.

[30] At the surface, the AI front (Figure 9) is evidenced by a typically very sharp increase in WVMR (e.g., from 4 to 12 gkg^{-1} on 13 June,) and wind speed (e.g., from 2 to ~7 ms^{-1} on 13), a change in wind direction, and drop in temperature (of ~2 K). Subsequently, winds are markedly more turbulent, consistent with a lack of surface decoupling. Arrival time of the AI does vary between about 01:00 UTC and 04:00 UTC, broadly consistent with estimates by *Grams et al*. [2010] of a mean speed of 10 ms^{-1} over the ~400 km from the coast to SS2 following initiation at ~16:00 UTC.

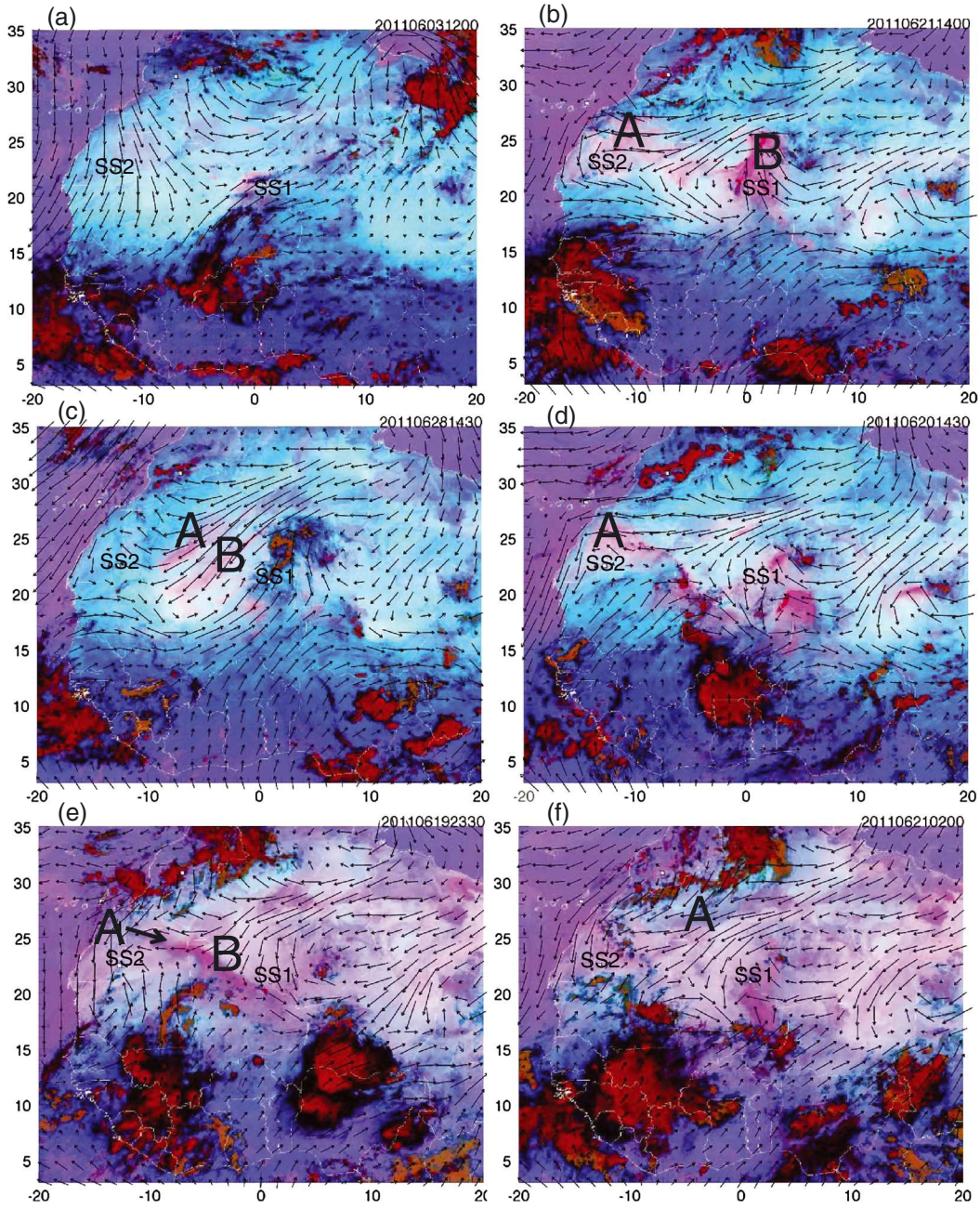

Figure 7. Exemplar cloud (red-black color tones) and dust aerosol (pink color tones) conditions over the Sahara during Fennec IOP 2011 from SEVIRI false color dust product. 925 hPa winds from ERA-Interim reanalyses are overlaid. (a) Low aerosol conditions during Maritime phase 12:00 UTC on 3 June. (b) Heat low phase, 21 June 14:00 UTC. Feature A is LLJ-related dust emission from north of SS2, (Feature B is a cold pool over SS1, see *Marsham et al*., [2012]). (c) Heat low phase, 28 June 15:30 UTC. Features A and B are dust emission from lacustrine deposits. (d) Heat low phase, 20 June 15:30 UTC. Feature A is small-aged cold pool. (e) Heat low phase, 19 June 23:30 UTC. Feature A is small active cold pool; B is aged cold pool. (f) 21 June at 02:00 UTC. Feature A is cold pool from Atlas Mountains. SS1 and SS2 are marked in Figure 7a only.

[31] Thus, the AI acts to create a rather complex nocturnal structure in the lower layers at SS2. The nocturnal surface temperature inversion, weakly developed by 00:00 UTC (green lines in Figures 4a and 4b), is eroded by the intrusion of the cool shallow well-mixed AI, with implications for the structure of the LLJ described below. As a result, at night after the arrival of the AI, near-surface wind speeds remain relatively high and variable (Figures 6d and 15d), indicative of turbulence during the night, as a result of the absence of a strong surface temperature inversion and decoupling (yellow lines in Figures 4a and 4b).

[32] A more detailed case study of AI propagation, rather earlier in the day than normal on 17 June is facilitated by analysis of observations roughly along a north-south timeline transect from a dropsonde released some 300 km north of SS2 (during the "heat low survey" flight of the French

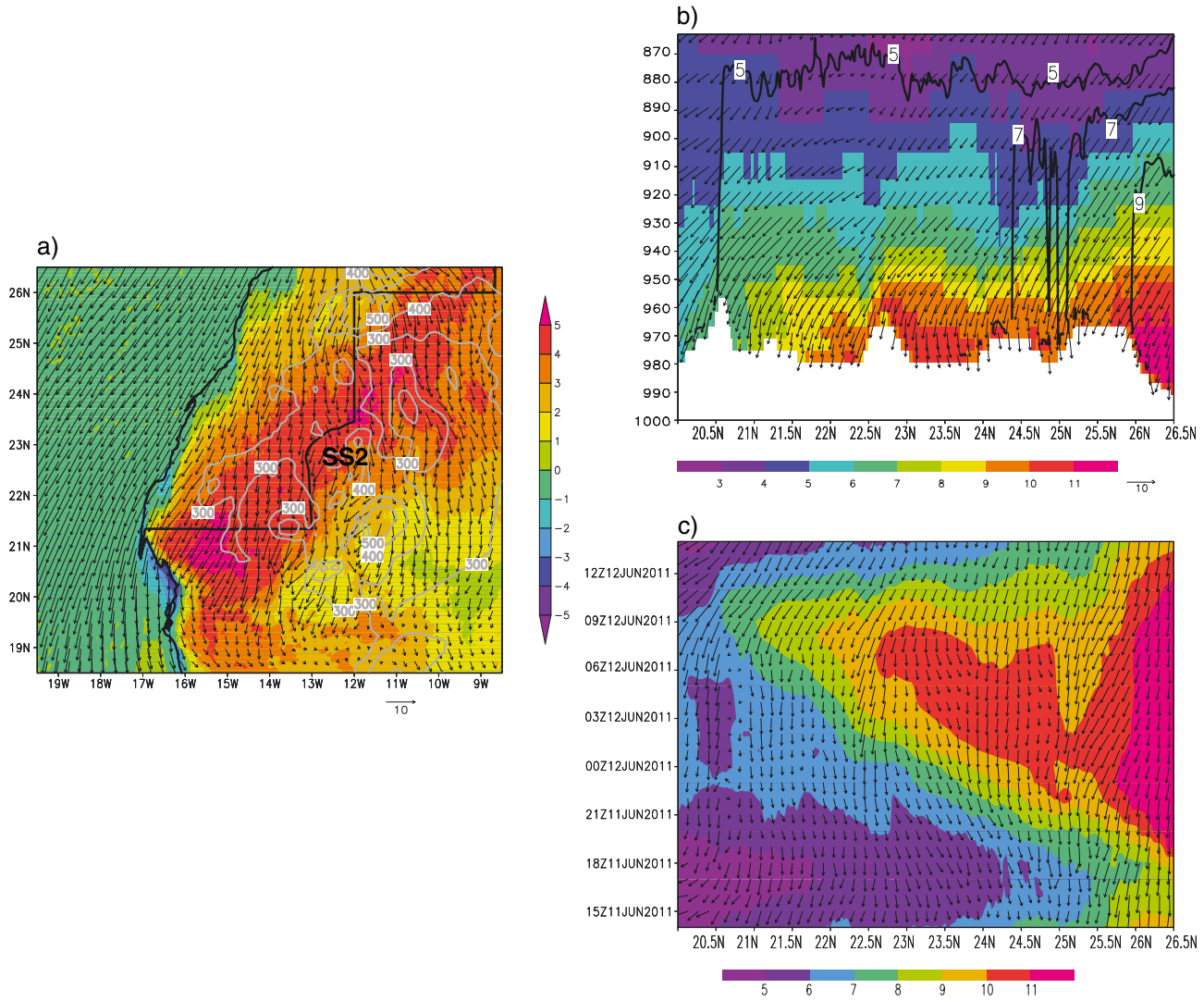

Figure 8. WRF simulation of Atlantic Inflow feature. (a) June 2011 mean 2 m specific humidity difference (gkg^{-1}) between 07:00 UTC and 15:00 UTC with 10 m winds at 07:00 UTC. (b) June 2011 mean specific humidity (gkg^{-1}) at 07:00 UTC (shaded) and 15:00 UTC (contours) with mean horizontal winds at 7:00 UTC for a north-south transect at 12.5°W. (c) Time-latitude plot of June 2011 mean diurnal specific humidity (gkg^{-1}) and 10 m winds for transect at 12.5°W.

research aircraft, Figure 9c), the Bir Moghrein Fennec weather station and SS2. The dropsonde at 18.22 UTC shows a well-mixed and rather deep (~800 m), cool (potential temperatures ~310 K), and moist (10 gkg^{-1}) layer with wind speeds up to 8 ms^{-1} characteristic of the AI. The inflow front was then evident at the Bir Moghrein weather station as a wind speed and temperature discontinuity at 20:00 UTC (no humidity data available, not shown). Arrival of the AI front at SS2 around 00:00 UTC on 18 June is evident from humidity increase from 6 to 11 gkg^{-1} and winds speeds of about 6 ms^{-1} (Figure 9b) and is evident in both the 00:00 UTC and the 06:00 UTC radiosondes as a moist, cool northwesterly layer of only around 100 m depth (Figure 5).

[33] The nocturnal increase in near-surface humidity is apparent on all days except 23 June when strong dry *Harmattan* northeasterly winds prevailed (Figure 6d). The sharp AI front can be detected on at least nine of the 20 days for which humidity data are available over the full diurnal cycle. On other days, a smooth nocturnal increase in WVMR occurs, consistent with accelerated flow towards the SHL across a mean WV gradient from the Atlantic inland. Combined, our surface and radiosonde data suggest that the AI front itself penetrates as far inland as SS2 on at least half of nights during the IOP. The time series of WVMR (Figure 6c) indicates that almost all the moistening of the lower troposphere at SS2 occurs at night, associated with the mean AI and the associated front. Calculation of vertically integrated moisture flux in the AI layer, defined as the layer below the temperature inversion, (average height = 158 m a.g.l.) from the 06:00 UTC radiosonde data, indicate a mean value of 8.6 $kgm^{-1}\,s^{-1}$ over the IOP.

[34] The AI as simulated by WRF (Figure 8) is consistent with these observations at SS2. SS2 is close to the inland limit of AI penetration (Figure 8a), and the magnitude of diurnal cycle in WVMR is at a maximum along a northeast-southwest axis over the western Sahara, passing over SS2, roughly parallel to the coast but around 300 km inland. The spatial extent of the AI indicated in Figure 8 is

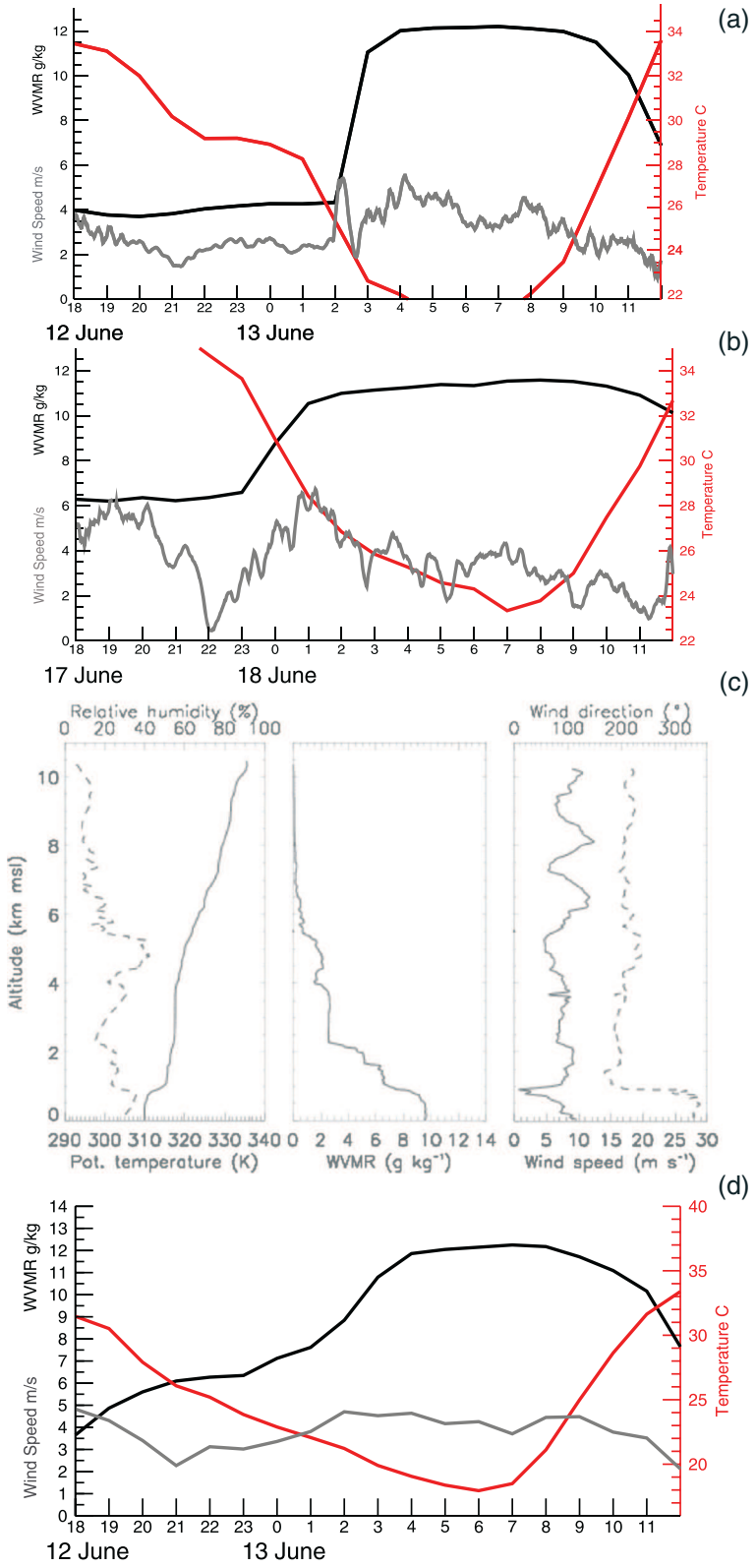

Figure 9. Evidence of two observed Atlantic inflow fronts propagating over SS2 and environs. (a) 12–13 June. (b) and (c) 17–18 June. Figures 9a and b show near surface conditions at SS2 where the left Y-axis shows near surface specific humidity (black line, gkg^{-1}) and wind speed (gray line, ms^{-1}), and the right Y-axis shows temperature (red line). Figure 9c shows vertical atmospheric profiles from FF20 dropsonde at 18.22 on 17 June 2011 at 26°N,11°W, of (left) potential temperature (solid line, K) and relative humidity (dashed line, %), (center) WVMR gkg^{-1}) and (right) wind speed (dashed, ms^{-1}) and direction (solid, degrees). Figure 9d as Figure 9a but from WRF simulation at 3 km horizontal resolution.

further confirmed by evidence of the shallow nocturnal mixed layer in radiosonde ascents from Tindouf (27.6°N, 8.1°W) in western Algeria (not shown). Figure 8c indicates the propagation of the AI inland from the coast of WA as north-northwesterly low-level flow initiating at ~17:00 UTC and reaching SS2 (22.75°N) in the early morning hours, consistent with the observations during at SS2. Comparison of the characteristics of the AI as simulated by WRF at different resolutions (3 km, 9 km, and other experiments at 27 km) indicates that the sharp AI humidity "front" apparent on many nights at SS2 (e.g., Figures 9a and 9b) can only be reasonable simulated at the highest 3 km model resolution (Figure 9d). Analysis of the global ERA-Interim reanalysis product (0.5 degree with 60 model levels) reveals that, despite the rather low 6-hourly resolution of the output fields, there is evidence of a well-mixed, humid near surface layer characteristics of the AI, which penetrates inland during the night, although at this spatial resolution the sharp AI humidity "front" is not well resolved (not shown). The depth of the AI layer at the location of SS2 at 06 UTC and the associated moisture flux integrated through the AI layer are also underestimated in ERA-Interim however by ~60%. Thus, the global model captures the essential structure of the AI but struggles to replicate precise detail, perhaps not surprisingly given that SS2 lies close to the inland limit of AI influence.

3.4. LLJ at SS2

[35] Nocturnal LLJs are commonly observed over desert surfaces worldwide (for a review see *Stensrud* [1996]) and over the Sahara in particular where they are responsible for a substantial proportion of dust emission [*Marsham et al*., 2012; *Schepanski et al*., 2009; *Todd et al*., 2008; *Washington and Todd*, 2005]. The existence of the LLJ is in essence the result of the diurnal cycle of surface heating and cooling in the context of a pressure gradient. Daytime insolation and sensible heating at the surface creates the hot, dry, and sometimes rather deep CBL observed at SS2. During the night, strong radiative cooling stabilizes the very lowest layers and effectively decouples most of the PBL from surface friction [Figure 4a; *Todd et al*., 2008] leading to an inertial oscillation around the equilibrium geostrophic wind [*Blackadar*, 1955; *Van de Wiel et al*., 2010] with supergeostrophic LLJ winds, which in the Sahara peak in strength before sunrise. After sunrise, surface heating causes the PBL to grow in depth and mixes momentum from the jet level down to the surface creating the distinctive surface peak winds (and dust emissions) from morning to midday observed in many Saharan locations [*Marsham et al*., 2011, 2012; *Todd et al*., 2008; *Schepanski et al*., 2009]. It should be noted that the degree of surface decoupling critically depends on factors suppressing turbulence near the surface during the night. At SS2 (Figures 5d and 5e) the LLJ is clearly evident below ~1000 m a.g.l. on most nights with (northeasterly) wind speeds peaking at 06:00 UTC typically ~6 ms^{-1} greater than the layer immediately above. However, the characteristic out-of-phase diurnal cycle of LLJ and surface winds is not strongly evident at SS2 (Figures 5d and 6d and section 3.6), although there is a small mean wind speed increase of about 1 ms^{-1} after 06.30 UTC. This apparent paradox of the existence of LLJ without a strong morning peak in surface winds results from the existence of the AI which (i) maintains higher near-surface wind speeds at night (~5 ms^{-1}) (ii) acts to suppress the decoupling of the surface from the CBL of the previous day leading to a weaker LLJ. As such, the AI undercuts the LLJ, and the LLJ is decoupled not from the surface but from the cooler and shallow AI layer below (see sections 3.4 and 3.6). The LLJ is therefore mixed slowly to the surface, resulting in prolonged moderate peak winds and relatively little dust emission, since dust uplift is a non-linear function of wind speed beyond some surface-dependent threshold.

[36] Day-to-variability in the nocturnal LLJ is, however, pronounced (Figure 5d). During the Maritime phase (6–12 June), the LLJ was a regular but relatively shallow and weak feature extending to about 600 m a.g.l. with maximum speed in the jet core at about 400 m a.g.l. of ~9 ms^{-1}. Subsequently, during the heat low phase, the LLJ was more variable as a result of synoptic-scale variability in regional pressure gradients associated substantially with the evolution of heat low and AEW toughs. On 16, 21–23, and 30, the LLJ was a deeper (core height >1000 m a.g.l) and stronger feature (exceeding >15 ms^{-1}) as a consequence of strong northeasterly flow around the surface SHL trough. This strong northeasterly LLJ was also observed to the north of SS2 close to Bir Moghrein on 21 and 22 June from dropsondes released before 0900 UTC (around the time of LLJ break down) from Fennec heat low survey flights FF22 and B607, respectively, with core wind speeds in excess of 25 and 18 ms^{-1}, respectively (Figure 10). In the former case (Figure 10a), the LLJ was likely overlying strong near-surface winds associated with a cold pool gravity current which had spread south from convection over the Atlas Mountains some 500 km to the north during the night. These largest LLJ events generated dust over northern Mauritania (section 3.5). On other days, the LLJ was weaker (14 and 18 June) or absent (28–29), when regional pressure gradients are weaker. Mostly, the LLJ has a meridional northerly component, although on a few days, a southerly LLJ is apparent (e.g., 21 and 25 June), when the influence of southerlies around the surface troughs penetrates as far north as SS2.

[37] The high moisture flux in the LLJ core (Figures 5b, 5d, and 5f), except in cases of the dry *Harmattan* LLJ, suggests the LLJ plays an important role in the moisture budget of the western Saharan, as it does in the Sahel and southern Sahara [*Parker et al*., 2005; *Lothon et al*. 2008]. Calculation of vertically integrated moisture flux in the LLJ layer, defined as the layer from the top of the AI to the height of wind speed minima above the LLJ core (average depth of 642 m) from the 06:00 UTC radiosonde data, indicates a mean value of 34.0 $kgm^{-1}\,s^{-1}$ over the IOP. These detailed observations provide the benchmarks for evaluation of weather-climate models. As an initial analysis of the performance of global models, ERA-Interim reanalysis data, for example, underestimate the mean nocturnal peak in low-level moisture and the LLJ core wind speed magnitude by about 30% and 20%, respectively. The bias in ECMWF operation analyses is slightly larger. In detail, although ERA-Interim (and ECMWF operational analyses) reveals a slight weakening of the LLJ between 00:00 and 06:00 UTC at SS2, perhaps as a result of the AI-LLJ interaction (section 3.3), the magnitude of this effect is underestimated and ERA-Interim (and ECMWF operational analyses) actually overestimates the LLJ in the lowest layers 06:00 UTC, whilst underestimating the LLJ during the night (see the mean diurnal cycle of ERA-Interim bias in

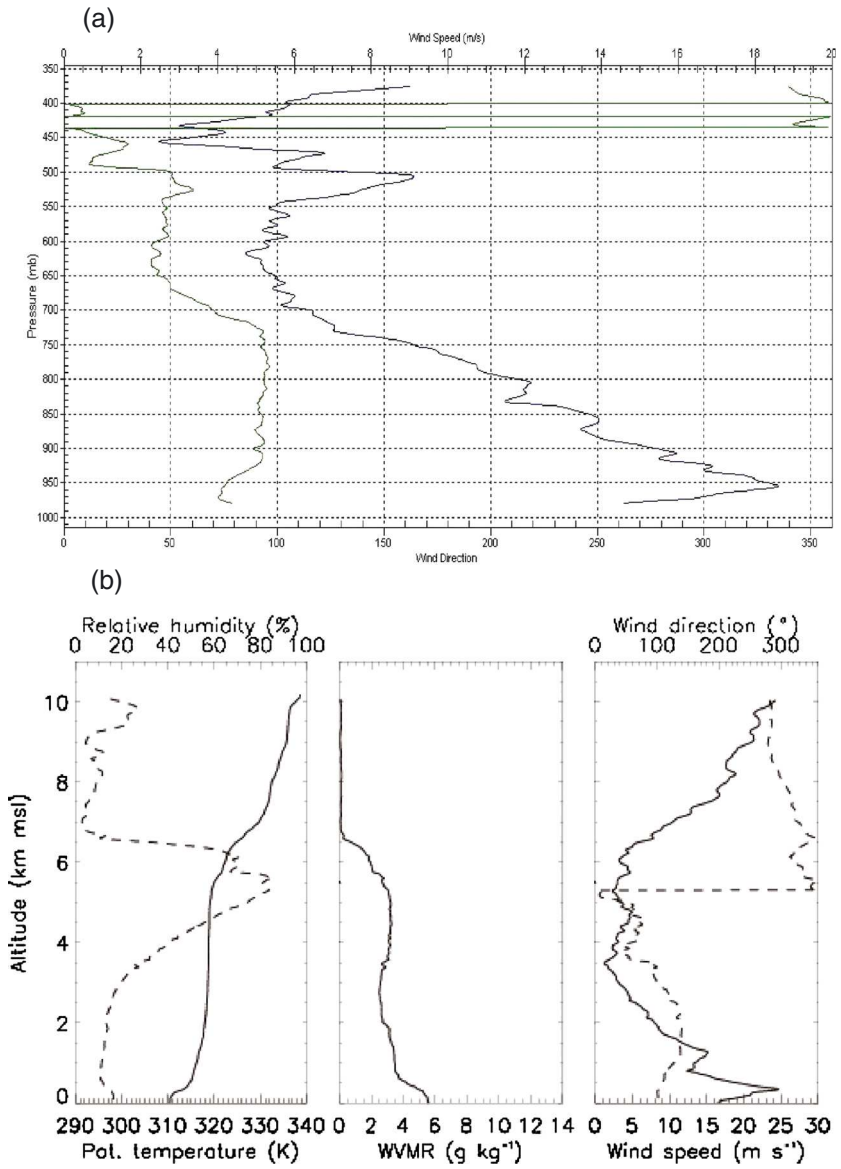

Figure 10. LLJ features observed from Fennec research aircraft. (a) Vertical profiles of wind speed (blue line, ms^{-1}) and direction (green line) from B607 dropsonde at 09:05 UTC on 22 June 2011 at 24.4°N, 10.25°W. (b) Vertical profiles of (left) potential temperature (solid line, K) and relative humidity (dashed line, %), (center) WVMR gkg^{-1}) and (right) wind speed (dashed, ms^{-1}) and direction (solid, degrees) from FF22 dropsonde at 07.59 on 21 June 2011 at 26°N,11°W.

Figure 16g, discussed in section 3.6). By way of comparison with other parts of the Sahara, the most extensively studied LLJ feature in the Sahara is that over the Bodele depression in northern Chad. *Todd et al*. [2008] and *Haustein et al*. [2012] note that the global NCEP reanalysis and Final Analysis product underestimates the magnitude of by about 50–60% but that higher resolution regional models can provide estimates of peak LLJ wind speeds within ~20%.

3.5. Dust Aerosol Conditions at SS2

[38] Analysis of long-term SYNOP data at Zouerate in a previous study [*Klose et al*., 2010] reveals relatively frequent reports of dust throughout the year with peak in both the winter and summer seasons, indicating that, broadly speaking, Zouerate is influenced by both the winter "Harmattan" dust process and the summer monsoon trough-related processes. Regarding the latter, dust reports peak in late summer, and June is a month of relatively low dust reports. During June 2011, aerosol loading over SS2 (Figure 6g) and the wider western Saharan domain (Figures 7 and 11) broadly reflects the transition between the Maritime and heat low phases over the Fennec IOP 2011. Aerosol Optical Depth (AOD) retrievals from the Multi-angle Imaging SpectroRadiometer (MISR) indicate a westward shift in elevated total-column aerosol loadings from the first to the second half of June 2011 (Figure 11). It should be noted that SS2 lies at the periphery of Saharan dust activity during the IOP. Nevertheless, during the Maritime phase, remarkably low AOD values were observed over the western Saharan sectors (Figures 7a and 11a) and specifically at SS2 where AOD

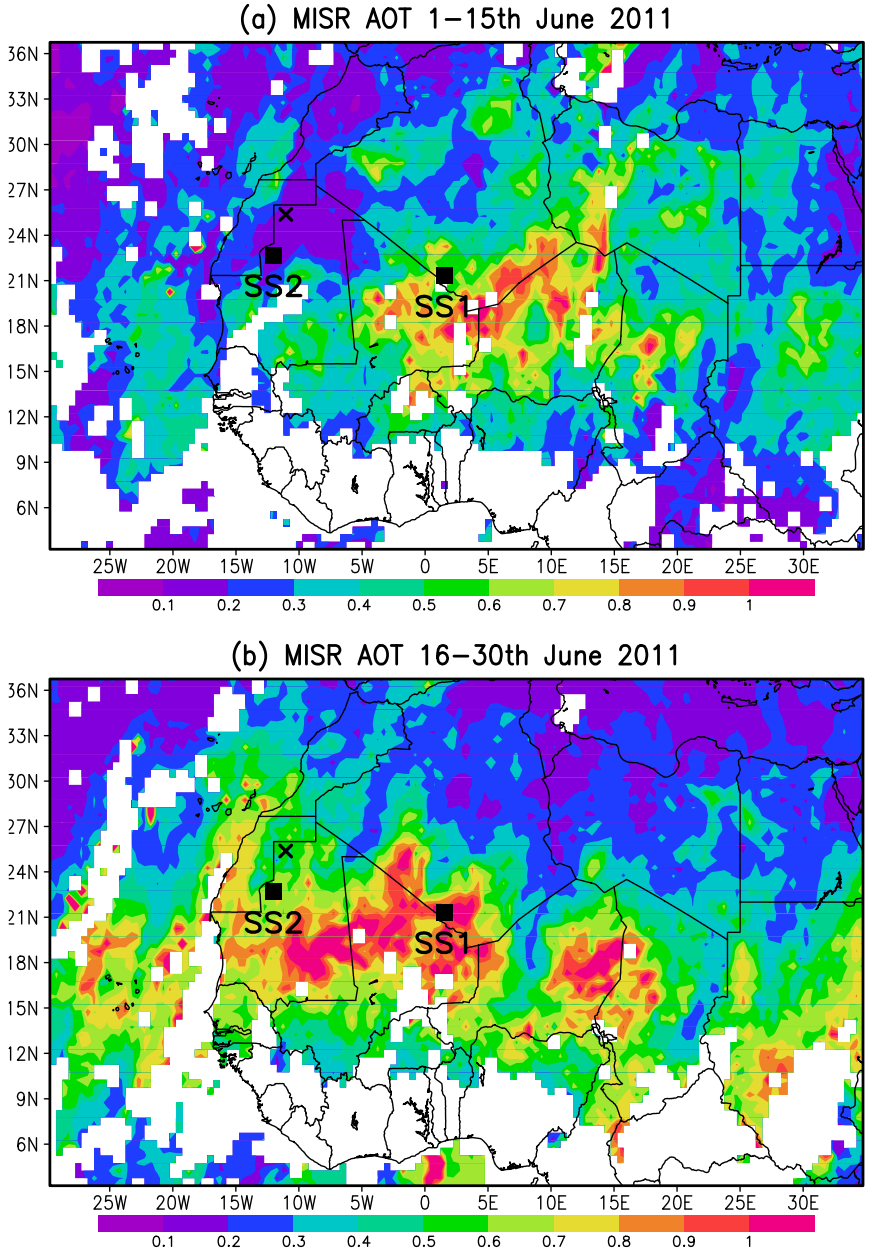

Figure 11. Mean AOD from satellite MISR observations averaged over (a) 1–15 June 2011 and (b) 16–30 June. Locations of SS1 and SS2 are shown with squares and Bir Moghrein with a cross.

values were persistently <0.2 (Figure 6g). At this time, near the longitude of SS2, the vertical section of Total Attenuated Backscatter from the CALIOP (Figure 12a) shows clear air at Saharan latitudes (~20–27°N) and significant aerosol restricted to areas south of ~15°N, in an elevated layer undercut by the strong maritime northwesterly flow (Figure 2b). Analysis of SYNOP "present weather" reports from the WMO station at Zouerate (only available during daytime) indicates no dust-related codes over the period 1–18 June.

[39] In contrast, during the heat low phase, elevated AOD values (>1) extended over the wider western Saharan sector of Mauritania-Mali (Figure 11b) and at SS2 AOD rose gradually from 13 June with peak values of >1.0 on 21 and 23 June and a peak of >2.5 on the afternoon of 30 (Figure 6g). Partitioning local emission and transport from remote sources at SS2 is problematic, but the SYNOP reports at Zouerate are instructive. During the 12-day period following 19 June, more than half of all present weather reports indicate a dust code. Of these, 73% were code 6 ("widespread dust") indicative of dust advection from other sources, which were recorded on 19, 21, 23, 25–27, 29, and 30 with visibility <10 km. The time series of these SYNOP reports are consistent with day-to-day peaks in AOD (Figure 6g). Weather codes indicating local dust emission were reported on three days (06:00, 09:00 UTC 21 June, with SYNOP westerly winds of 7–8 ms^{-1}; 12:00, 15:00, and 18:00 UTC 23 June, with northeasterly winds of 8–10 ms^{-1}; and at 12:00, 15:00 UTC 29 June, with easterly winds of 8–9 ms^{-1}) all of which are the dust code 7 (raised dust but not a dust/sand storm) except code 32 (dust storm) at 12:00 UTC on 21. Lack of

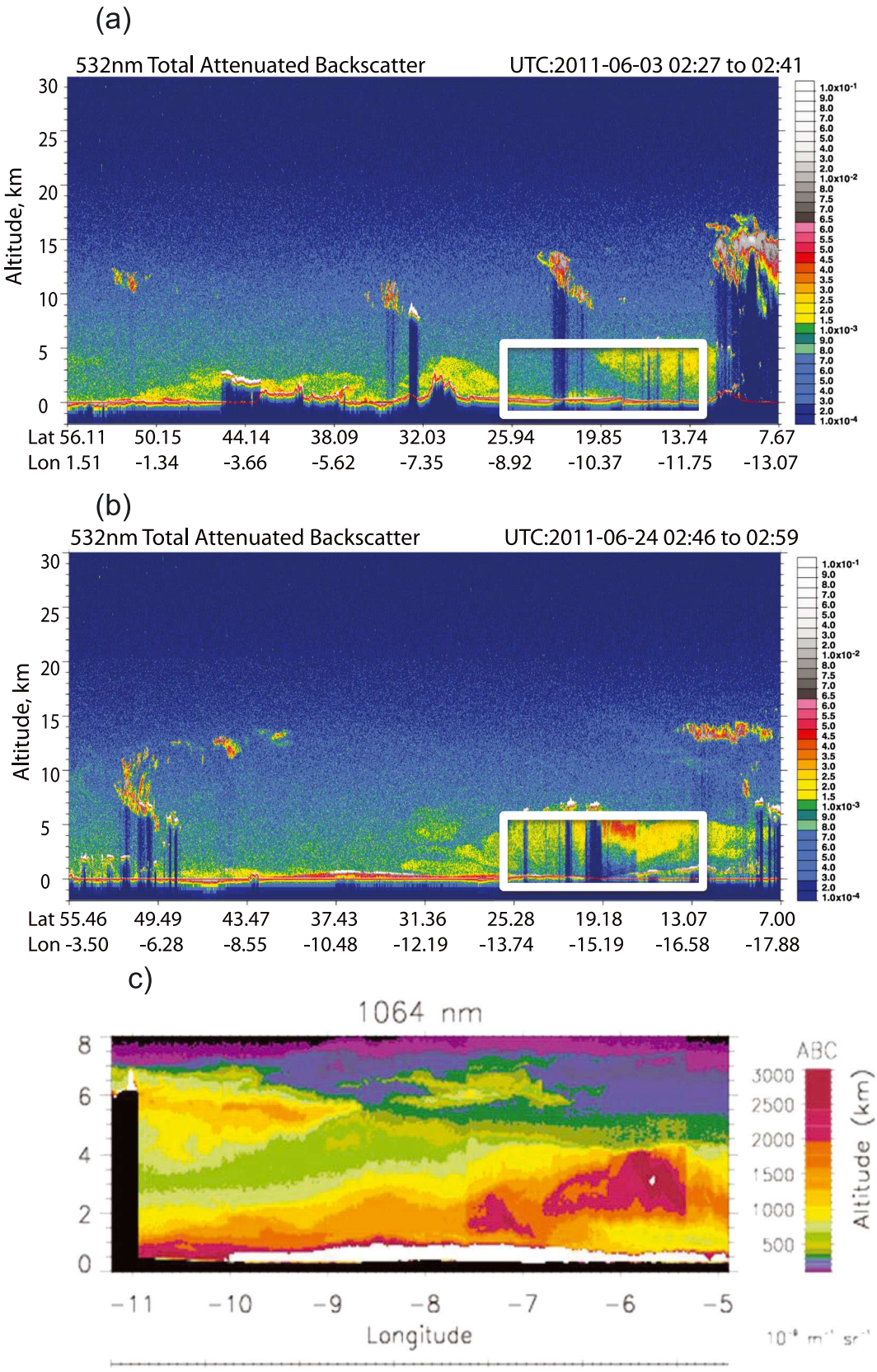

Figure 12. (a) and (b) CALIOP lidar backscatter profiles over the west coast of Africa (Saharan sector indicated with a white box) indicative of the "maritime" phase on 3 June 02:46 UTC and the "heat low" phase on 24 June at 02:46 UTC. (c) Lidar backscatter from airborne instrument on FF22 at 08:00–08:30 UTC on 1 June. Dust layers and inferred sources are marked.

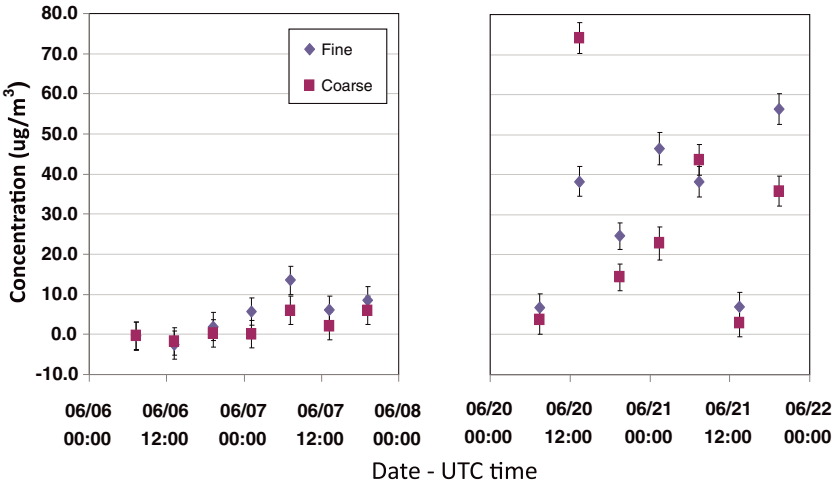

Figure 13. Aerosol mass concentration derived from LASS filters collected at Bir Moghrein (ug/m^3) for fine (diameter < 2.5 m) and coarse (2.5 m < diameter < 10 m) particles. Left: Days 6 and 7 June (Maritime phase) and Right: Days 20 and 21 June (heat low phase) for coarse (in red) and fine (in blue) filters.

high time-resolution surface data at critical times on these days prevents clear analysis of dust emission wind speed thresholds. 23 June is a particularly interesting case with a strong northeasterly *Harmattan* LLJ and also deep moist convection present over SS2 in the afternoon with gusty winds, suggestive of downdrafts from convection, reaching 15 m/s around midday (the maximum observed at SS2), such that both the LLJ and downdrafts may be responsible for dust emission. Interestingly, occasionally during the Maritime phase of the IOP, winds exceeded values observed on 21 and 29, but no emission was reported (Figure 6d), a paradox that cannot easily be resolved without direct observations of dust emission. There were no reports of the more significant code 9 (dust/sandstorm) at SS2 during the IOP.

[40] Analysis of SEVIRI dust products indicate that elevated dust loadings during the heat low phase relate primarily to dust advected over SS2 in the *Harmattan* low-level flow from dust sources upstream. Precise identification of these source regions, given the time lags involved in long-range transport and the variety of sources and emission mechanisms over the heat low sector (see *Marsham et al.*, [2012]), is a substantial task, which is being investigated in the Fennec project, and we expect to be documented in publication. However, from backtracking plumes in SEVIRI, we can infer that most of the dust observed at SS2 was generated by northeasterly *Harmattan* LLJ events.

[41] The heat low phase exhibited a strong easterly and northeasterly synoptic-scale flow over central Algeria, northern Mali and Northern Mauritania, around the northern flank of the heat low and AEW troughs (Figure 3b). Dust emission typically results from elevated surface winds as the nocturnal LLJ mixes to the surface in the mid morning. Dust emission from this mechanism is apparent from SEVIRI data over northern Mauritania on 21, 23 and 28–30 June (Figures 7b, 7c, and 12c), largely explaining the peaks in observed AOD (Figure 6g). The case of 21 June is interesting because the airborne lidar from Fennec flight FF22 (Figure 12c) shows a near surface dust aerosol layer resulting from a southward moving cold pool which was subsequently augmented by LLJ-related emission later that day (Feature A in Figure 7b). It is interesting to note that the Fennec research aircraft flights B600 and B601 on 17 June 2011 observed high dust concentrations associated with a similar northeasterly LLJ event over Northern Mali with exceptionally large size distribution [*Ryder et al.*, 2013], although the trajectory of this dust plume was slightly to the south of SS2. In addition, strong dust plumes were detected from preferential source regions including the palaeo lacustrine deposits at 24.5°N, 5.5°W, in the extreme Northwest sector of Mali and those at ~26.5°N, 1.5°E west of In Salah, central Algeria, most notably on 27–29 June (Figure 7c). Rates and precise trajectories of southwestward transport of dust plumes from these sources vary, but typically dust is advected largely to the south of SS2 after dark and so is not apparent in the AERONET observations at SS2. Such dust emission in strong northeasterlies is advected towards the coast of West Africa and is mixed vertically throughout the CBL and into the SRL, exemplified in Figure 12b from 02:46 UTC on 24 June clearly indicating the plume emitted over Mauritania on 23 described above. The contrast in large-scale dust loading at the latitudes of the Sahara between the maritime and heat low modes is evident from comparison of Figures 12a and 12b.

[42] A major mechanism of dust emission during summertime in the central Sahara is the high wind speeds generated by cold outflows from MCSs. These dust fronts (*haboobs*), which typically move northwards from nighttime convection over the Sahel (and central Sahara), are known to be responsible for a substantial proportion of dust emission in the Southern and central Sahara [*Marsham et al.*, 2012]. Dust from these events can persist over the Sahara for many days following emission and substantially explains the existence of the mean WA aerosol hotspot over the central Sahara in summer [*Knippertz and Todd*, 2010; *Marsham et al.*, 2008; Figure 1]. However, SS2 is rather too far north and east of the main locus of mesoscale convective activity to be frequently influenced by cold pool features from the south. However, convective cold pools influence SS2 in the following cases; (i) 23 June (see above) when local recorded dust emission is at least in part associated with downdrafts from moist convection over SS2 leading to the maximum observed wind speeds, and due to the non-linear nature of dust uplift

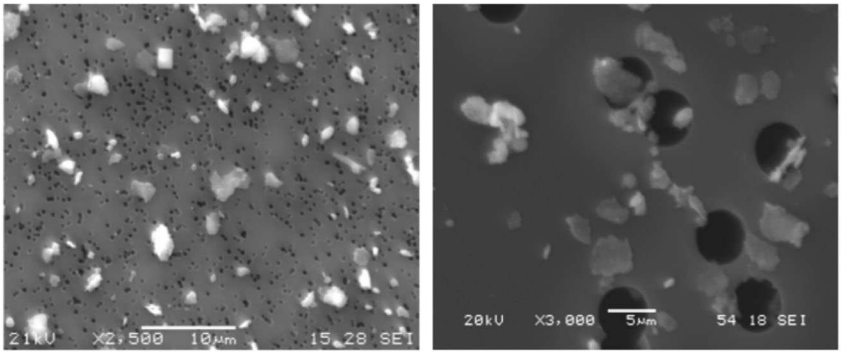

Figure 14. SEM images of Nuclepore filters with fine (left) and coarse (right) aerosol particles collected using the LASS instrument at Bir Moghrein during the period of 19:00–01:00 UTC between 20 and 21 June.

possibly a significant fraction of the local emission during June 2011. (ii) 20 June when an aged cold pool dust plume can be identified at SS2 (Feature A in Figure 7d) whose source was a large *haboob* initiated over central Mali in the early hours of 19 June. The responsible MCS developed in the southerly monsoon surge around a trough centered over eastern Mauritania (Feature B in Figure 7e).(iii) Night of 20–21 June when a southward propagating *haboob* from convection over the Atlas Mountains reaches the environs of SS2 late on 21, persisting until morning 22 (Figures 7f and 12c). (iv) Early hours of 20 June a much smaller cold pool feature was observed propagating from convection over coastal Southern Morocco on the night of 19–20 June arriving at SS2 in the (Figure 7e), but with limited dust loadings.

[43] Results from in situ sampling of dust collected by the LASS in Bir Moghrein highlight the contrast between the Maritime phase and heat low phase. Figure 13 shows the mass concentration of aerosol particles in units of µg/m^3 of air, collected on days 6 and 7 June (Maritime phase) and on days 20 and 21 June (heat low phase). Concentrations were calculated based on the mass collected on the Nuclepore filters and on the volume of air sampled during every 6 h period starting at 07:00 UTC. Each value in the plot is associated with the initial time of sampling, although the concentration represents an average for the whole 6 h period of sampling. During the Maritime phase period, very clean conditions were observed, with fine and coarse mode concentrations below 10 µg/m^3 and close to the detection limit or our technique, except for the morning of 7 June where this concentration is slightly larger. During the heat low phase, the observed concentrations vary from 5 to 70 µg/m^3 with oscillations in the predominance between the fine and coarse modes along this period. Figure 14 shows two Scanning Electron Microscopy (SEM) images of a fine and a coarse filter collected between 19.00 UTC on 20 and 01.00 UTC on 21 June. SEM images show in black the circular pores of the filter, with particles collected on its surface on a lighter color. Coarse filters have pores of 5 um, and they were used to retain particles with size mostly smaller than 10 um. Fine filters, positioned after the coarse filter, were used to collect particles with size mostly below 5 um. Figure 14 shows asymmetrical particles with a large variety of shapes. Further image analysis will be applied to obtain particles size distribution.

[44] Estimating the effect of dust (and cloud) on the radiation budget is compromised by a lack of downwelling shortwave flux data in the latter days of the IOP (Figure 6d). During the heat low phase, a complete set of daytime data is only available on 26, with cloud-free conditions. On this day, observed AOD of ~0.5 coincided with peak downwelling shortwave flux values about 100 Wm^{-2} lower than the days during the Maritime phase, (differences due to solar zenith are marginal at this time of year). Therefore, we make an estimate that enhanced aerosol loadings influence the surface radiation budget such that downwelling shortwave fluxes decline by ~200 Wm^{-2} per unit AOD, comparable to that at SS1 where analysis was further complicated by cloud [*Marsham et al.*, 2012]. This is more than the figure of 140 Wm^{-2} per unit AOD during the major dust event of

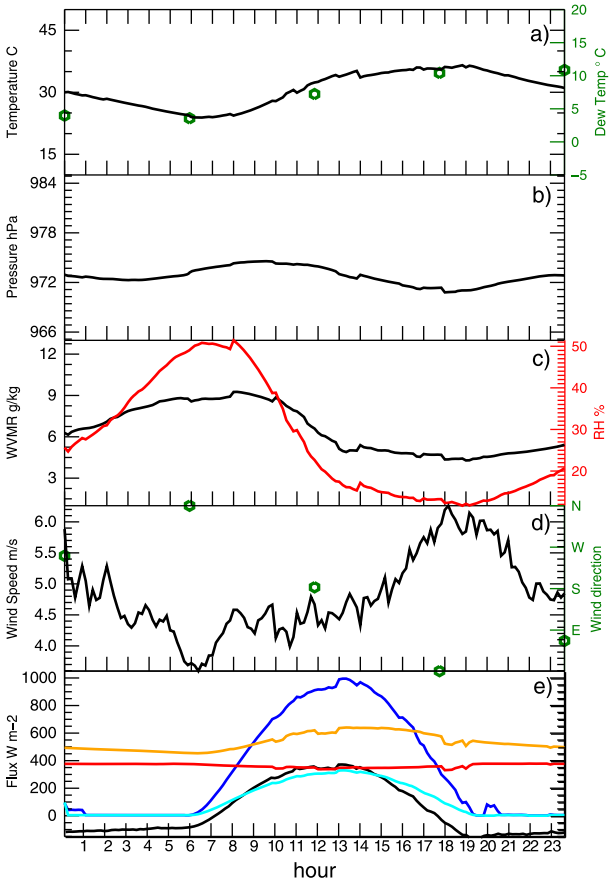

Figure 15. As Figures 6a–6e but for the mean diurnal cycle.

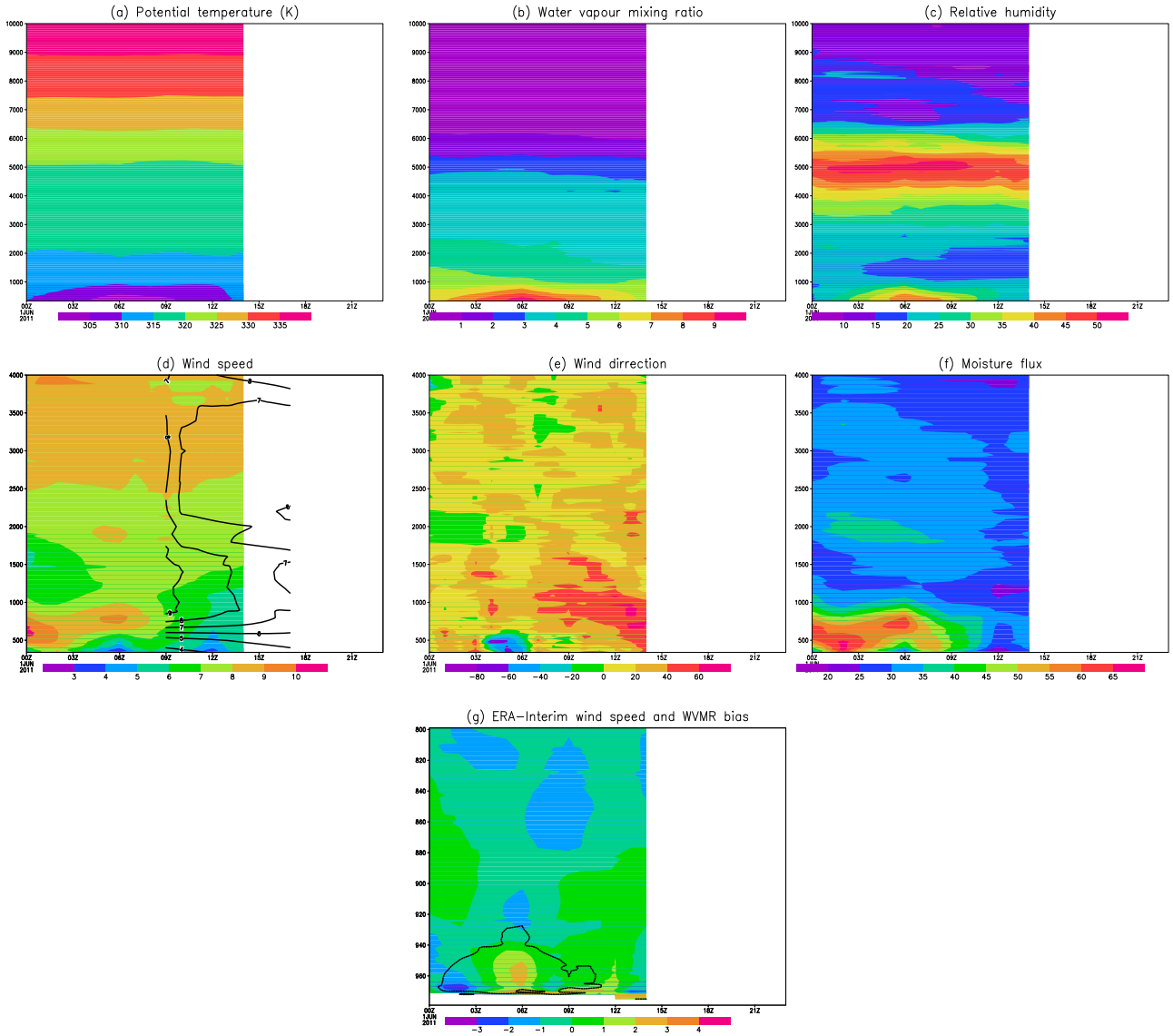

Figure 16. Mean diurnal cycle at SS2 of the vertical profile of (a) potential temperature (K), (b) WVMR (gkg^{-1}), (c) relative humidity (%), (d) wind speed (ms^{-1}) from radiosondes (shaded) and pibal (contours) observations, (e) wind direction (degrees from north), (f) WVMR flux ($gkg^{-1}\,ms^{-1}$), (g) bias in ERA-Interim reanalysis wind speed (shaded, ms^{-1}) and WVMR (-2 gkg^{-1} contour), with respect to radiosonde data (ERA-Interim is interpolated to 1 hPa in the vertical). Note different height ranges in Figures 16d–g compared to Figures 16a–c.

March 2006 [*Slingo et al.*, 2006] For this case, *Milton et al.* [2008] demonstrate that the inclusion of dust aerosol processes in a Numerical Weather Prediction reduced the large model bias in radiation fluxes considerably. Similarly, analyses of cloud radiative effects are problematic due to very limited radiation data in the heat low phase.

3.6. The Mean Diurnal Cycle

[45] Mean diurnal cycles (derived from all available data during June 2011) at the surface and through the troposphere are shown in Figures 15 and 16, respectively. The mean diurnal cycle in many surface variables is strongly driven by the surface energy balance (Figure 15). Mean net radiation peaks at ~400 Wm^{-2} during the day and is around -100 Wm^{-2} at night, indicating a very large diurnal cycle of radiative heating and cooling. Net LW cooling varies from around 100 Wm^{-2} at night to ~290 WM^{-2} during daytime. Upward SW flux is around 31% of downward SW flux such that net SW heating peaks at almost 700 Wm^{-2} at local midday. Upward LW flux peaks at ~13:30 UTC, leading 2-m atmospheric temperature by ~2 h. Downward LW flux shows a maximum (minimum) at around 18:00 (06:00) UTC, reflecting the temperature of the overlying atmosphere and the diurnal cycle in cloud cover.

[46] The strong diurnal cycle in heating and cooling leads to a pronounced diurnal cycle in 2-m temperature with a maximum of ~36°C around 16:00 UTC and a minimum of ~24°C around 06:00 UTC (Figure 13a). The classic semi-diurnal cycle in surface pressure [*Pugh*, 1987] is apparent (Figure 15b). Unlike many other Saharan locations, there is

a relatively weak diurnal cycle of near-surface wind speed (Figure 15d). We interpret this as result of the lack of surface decoupling at night due to the AI (see section 3.4) which maintains relatively high nighttime surface wind speeds, limiting the strength of the LLJ at night (section 3.5) and providing a strong temperature inversion above the AI and below the LLJ, such that downward mixing of the LLJ in the hours after sunrise is relatively weak. The diurnal peak in near-surface winds at 19:00 UTC exists both in observations (Figure 15d) and in model simulation (not shown), at a time when wind speeds associated with turbulent eddies in the afternoon (see Figure 15d) would normally be expected to decrease, e.g., *Todd et al*. [2008]. We propose an explanation of this rather unusual diurnal cycle in surface winds from interpretation of the radiosonde and Pibal winds below.

[47] Radiosonde data are limited to the 00:00–14:00 UTC period so that we do not completely sample the diurnal evolution of vertical mixing in the SABL. Profiles indicate that overnight cooling occurs below about 2000 m (Figure 16a) with an increase in low-level wind speed associated with the nocturnal northeasterly LLJ (Figure 16d) peaking at $>10\,ms^{-1}$ at 00:00 UTC at about 400 m above the surface. The classic clockwise rotation over the diurnal cycle of the zonal and meridional components of wind in the LLJ core (and surface winds) noted in other studies [*Todd et al*., 2008; *Marsham et al*., 2012] is apparent here and confirmed from the WRF simulation (not shown). The LLJ peak at SS2 is, however, somewhat earlier and weaker than LLJs observed elsewhere, which peak just before sunrise. It seems that the weak morning peak in LLJ at SS2 results from the arrival of the AI in the early hours of the morning (mean northwesterly near surface flow at 06:00 UTC flow in Figure 16e), which acts to mix near surface and lowest atmospheric layers (e.g., yellow line in 4a) and to limit decoupling and further acceleration of the nocturnal LLJ (see also section 3.4), a process which may be underrepresented in the ERA-Interim reanalysis (and ECMWF operational analyses) data, as indicated by the overestimation of the LLJ by these models in the lowest layers (Figure 16g). Indeed, the height of the LLJ in observations actually rises slightly through the early hours as the AI layer deepens, a feature not captured by the models. The LLJ decays from the surface upwards after sunrise as the depth of the CBL deepens and turbulent mixing erodes the LLJ. Pibal data (contours in Figure 16d) indicate that the nocturnal LLJ actually persists at ~1300 m at 09:00 UTC, above the growing CBL. The CBL growth starts later at SS2 than other more continental locations due to its western position, and the growth rate slower due to the existence of the cool AI air, such that the LLJ decays most rapidly between 09:00 and 12:00 UTC. In the early afternoon, the growing CBL breaks through into this now elevated LLJ and mixes momentum to the surface maintaining elevated surface wind speeds through the afternoon (Figure 15d). As the CBL grows through the lower few km of the atmosphere, momentum from strong winds ($\sim$8–9 ms^{-1}) at heights of 2500–5000 m appears to be mixed downwards to the surface (note the decline in wind speeds at ~2000 m and the downward sloping wind speed contours below ~1000 m from pibals). This probably explains the peak in surface winds speeds at ~18:00 UTC, although we cannot rule out the effect of local topographic and albedo features.

[48] Regarding moisture, nocturnal mean moistening is evident at the surface (Figure 15c, the WVMR peak values of >9 gkg^{-1} occur at ~07:00 UTC and minimum values of ~4 gkg^{-1} at ~19:00 UTC) and in the lower layers (Figure 16b increases in WVMR from ~6 to ~9 gkg^{-1} from 00:00 to 06:00 UTC). We associate this cycle with both the mesoscale AI circulation and the nocturnal acceleration of flow towards the continental interior across the mean moisture gradient towards the central Sahara, described in more detail in section 3.3. The ERA-Interim (and ECMWF operational analyses, not shown) underestimates water vapor in the lowest layers by about 20–30% as shown in Figure 16g. There is an interesting distinction between the Maritime phase and heat low phase (not shown) in that the former experiences a rather deeper and uniform moist layer of some 500 m depth which may be indicative of the depth of the AI in this period.

[49] At SS2, cloud cover (Figure 15f), especially during the heat low phase, exhibits a strong diurnal cycle with generally cloud-free conditions through the morning and early afternoon, but rising sharply at ~15:00 UTC and peaking at ~20:00 UTC at which time mean cloud cover is 75%. This is associated with the development of shallow convection at the top of the SRL during days when mixing of water vapor occurs throughout the depth of the SRL/CBL and high relative humidity values at the top of the SRL are maximized.

4. Summary and Conclusions

[50] Lack of observations over the central Sahara sector has hindered our understanding of the dynamical and thermodynamical processes in this large region, and therefore both climate and NWP model skill is often limited in this region and beyond. This is particularly important during the boreal summer months when the SHL and aerosol maxima are most fully developed and interactions with the West African Monsoon most significant. The project "Fennec: the Saharan climate system" sought to fill gaps in our observations with a comprehensive set of surface and upper air observations from ground and aircraft-based instrumentation. This paper summarises the key findings from ground-based observations at Fennec SS2 at Zouerate, Mauritania in the Western Sahara during the IOP of June 2011. We are able to quantify and provide uniquely fine detail on some of the key processes associated with diurnal to seasonal-scale evolution of the western Saharan atmosphere, notably ventilation and humidification of the western Saharan region and the SHL associated with a range of meso- and synoptic-scale processes.

[51] During the IOP of June 2011, SS2 and the western Saharan region experienced a rapid transition around 14 June from what we refer to as a Maritime phase to a heat low phase with markedly contrasting atmospheric and aerosol conditions. The Maritime phase is characterized by a SHL displaced to the east of the mean June position, such that the western Saharan region experiences a strong regional-scale maritime influence, driving large-scale cold advection throughout the lowest ~4 km of the troposphere into a rather large swath of the western Saharan region. This maritime air has very low aerosol loadings. In contrast, during the heat low phase, the SHL is shifted westward to lie close to or westward of its June climatological position and the western Saharan region is essentially hot (>10 K warmer than the

Maritime phase at 800 hPa) and dusty, with the westward advection of the SRL over SS2. In both the Maritime phase and heat low phase, the CBL develops during the day with PBL heights of around 1500 m at 12:00 UTC. During the Maritime phase, the CBL at 900 hPa is around 15 K cooler than during the heat low phase. During the heat low phase, the CBL remains cooler than SRL, but over time heating allows the development of a nearly well-mixed CBL on occasions throughout the lowest ~5 km of the atmosphere (observed only during the early afternoon descent of the 12:00 UTC radiosonde release, and in dropsonde data from the Fennec research aircraft "heat-low survey" flights to the northeast of SS2).

[52] The influence of this transition between these Maritime and heat low phases was felt across the western and central Sahara as reflected in observations at Fennec SS1 [*Marsham et al*., 2012], In addition, the transition between these Maritime and heat low phases at SS2 is consistent with the timing of the mean northwestward seasonal migration of the WAHL and its summertime transition to the western Saharan region at which point it can be termed the SHL [*Lavaysse et al*., 2009]. Analysis of data from June 2011 [*Roehrig et al*., 2012] indicates an onset date for the West African Monsoon itself of 13 June 2011 following the Maritime phase (the "heat low east" phase). It remains to be fully determined what role intraseasonal variability and extra-tropical disturbances play in this transition and/or extent to which the observed transition is tied to the mean seasonal cycle in the region. The Maritime phase/heat low phase transition during the Fennec IOP at SS2 is congruent with a phase shift in the intraseasonal east-west heat low mode of *Chauvin et al*. [2010] and highlights the role of the midlatitude circulation in modulating conditions across the entire Sahara and beyond, an intriguing focus for further work on intraseasonal predictability.

[53] A number of processes observed at SS2 operate at the diurnal timescale, notably the AI and the nocturnal LLJ. The AI, a shallow north-northwesterly meso-synoptic-scale circulation, is evident at SS2, arriving in the early hours of the morning on about 60% of nights during the IOP. The AI plays an interesting role in the regional climate by cooling and moistening the western flank of the western Saharan sector. At SS2 during the IOP, all moisture increases are nocturnal, associated with both (i) the AI feature, although an AI "front" is not always observed and (ii) the nocturnal LLJ, typically considered the primary mechanism of nocturnal humidification [*Peyrille and Lafore*, 2007], from which moisture is mixed to the surface by 09:00 UTC and subsequently into the CBL. Mean moisture flux vertically integrated over the LLJ layer ($34\,kg\,m^{-1}\,s^{-1}$) was around four times higher than in the AI layer ($9\,kg\,m^{-1}\,s^{-1}$). From model simulations and contextual data from aircraft, we infer that SS2 is close to the limit of inland penetration of the AI front. However, during the heat low phase, the LLJ was often a dry feature advecting hot, dry Saharan air southwestward such that the role of the AI in ventilating and humidifying the SHL is relatively greater. Overall, moisture flux over SS2 was higher during the Maritime phase than during the heat low phase.

[54] At SS2, there was little evidence of monsoon intrusions or convective cold pools, in contrast to Fennec SS1 further east [*Marsham et al*., 2012]. Thus, the central Sahara received moisture primarily through the nocturnal monsoon surge and "haboobs" whilst the western Sahara is moistened by the AI and nocturnal LLJ. Peak nocturnal low-level WVMR is about 30% higher at SS2 than SS1. Overall, our observations confirm the nocturnal humidification at low levels of the western Saharan region and the subsequent vertical turbulent mixing through the SABL during the afternoon (most pronounced during the heat low phase), recognized previously from model simulations and analyses.

[55] There is an interesting interaction between the AI and LLJ. The AI acts to limit the nocturnal decoupling of surface from the overlying near-surface layers, which in turn weakens the strength of the LLJ feature. The nocturnal LLJ was observed on almost all nights, but due to the effect of the AI, peaks at 00:00 UTC rather than just before sunrise as observed elsewhere. The magnitude and depth of LLJ core are also notably lower than those observed at SS1 [*Marsham et al*., 2012] and elsewhere in the Sahara. Weaker surface decoupling and a strong inversion over the AI further damps the diurnal cycle of near-surface winds, and by implication, the potential for LLJ-related dust emission events. Nevertheless, local dust emission at SS2 occurs during cases of enhanced *Harmattan* LLJ-mixing events associated with strong pressure gradients around an intensified SHL trough. Relatively slow growth of the CBL through the cool AI means that the LLJ persists until the 09:00–12:00 UTC period. During the afternoon the CBL then grows into stronger winds above 2500 m mixing momentum to the surface creating the maximum at 18:00 UTC.

[56] Aerosol loading over SS2 is generally substantially lower than at SS1 further east, confirming SS2 as close to the northwestern limit of the WA dust "hotspot" feature. Dust events in the region are restricted to the heat low phase when dust advection occurred on many days, from sources upstream over Northern Mauritania and Algeria, activated primarily by strong *Harmattan* LLJ events and rapidly dispersed through turbulent mixing upwards through the CBL. Local dust emission was probably limited only a few such events. Our results highlight the potentially dominant role of LLJ-related emission in this northwestern SHL region, although emission is suppressed at SS2 and the maritime fringe of West Africa due the rather weak LLJ. Transport of dust from remote *haboob* features to SS2 was limited in comparison to SS1 as SS2 is too remote from the main locus of moist convection over the Sahel. Indeed, the coincidence of dust transport and strong *Harmattan* winds means that dust is exported rather quickly from the continent, further suppressing AOD values at SS2. During the IOP, the Maritime phase circulation (i) limits emission over the western Saharan region and (ii) maintains a Saharan dust plume transport trajectory further south and east over the tropical Atlantic than during the heat low phase, consistent with the mean seasonal northward migration of the Saharan dust transport plume over the Atlantic observed from satellite data (Ben-Ami et al., 2012). Prior to Fennec, case studies implicated a range of dust generation mechanisms (see *Knippertz and Todd* [2012] for a review), but the relative importance of each is as yet un-quantified. The unique Fennec data will allow major advances towards this goal.

[57] Overall, during fennec IOP, at SS2 in comparison to SS1, the SABL: (i) Is cooler during the day (by about 7 K near the surface and about 3 K at 2000 m) and night (by about

6 K near the surface and 1 K at 2000 m). (ii) Has shallower daytime PBL heights (<40% of SS1 values). (ii) Is more moist below 1000 m especially at night (by about 50% of SS1 values) and drier above 1000 m during the day (by about 10–20% of SS1 values) as a result of weaker vertical mixing of moisture. (iii) Has a substantially lower frequency of cloud cover. (iv) Has an ~10% weaker nocturnal LLJ maximum. (v) Is less dusty with mean AOD at SS2 less than 50% of that at SS1. The contrast between the Maritime and heat low phases is apparent at both SS1 and SS2.

[58] Qualitative experience of NWP model forecast evaluation during Fennec indicates that high-resolution (12 km) limited area models typically resolve well the location and magnitude of LLJ features at lead times of around 24–48 h, as well as the extent and structure of the nocturnal AI. Resolving the fine structure of the AI requires models with very high resolution. Nevertheless, our evaluation of the ERA-Interim and ECMWF operational analyses fields, exemplifying current global model capabilities, indicate that these global models are able to resolve well many of the key features of the circulation at SS2 and the wider western Sahara that are relevant to the processes of SHL ventilation including the LLJ and AI. However, the subtle detail, including the interaction of the LLJ and AI, remains elusive, and LLJ magnitudes and moisture fluxes are underestimated by many tens of percent. The causes of model biases require further sensitivity tests to model horizontal/vertical resolution and physical parameterisations. Comparison of the 60-level ERA-Interim and 91-level ECMWF operational analyses at SS2 indicates that increased vertical resolution in itself does not reduce nocturnal LLJ and humidity biases. Indeed, systematic evaluation of NWP errors and the contribution of data assimilation over the Sahara will be the subject of further Fennec papers. Fennec observations including those at SS2 provide a unique resource with which to evaluate the ability of the current generation of global climate models to resolve the detailed processes governing the SHL including large-scale phase shifts and the link to the midlatitude circulation as well as the associated processes of ventilation, moisture budgets, and aerosol interactions. This will further contribute to our understanding of the role the SHL plays in the regional climate system including the West African Monsoon itself.

[59] **Acknowledgments.** Fennec was funded by a UK NERC consortium grant (NE/G017166/1). We would like to thank ONM Mauritanie for operation of SS2, the AERONET, and PHOTONS teams for assistance with the Cimel sun photometer. CIMEL Calibration was performed at the AERONET-EUROPE calibration center LOA supported by ACTRIS (European Union Seventh Framework Program (FP7/2007–2013) under grant agreement no. 262254. False color SEVIRI imagery is taken from the Imperial College Fennec web site: http://www.fennec.imperial.ac.uk. Acknowledgement is made to the Facility for Ground-based Atmospheric Measurement, National Center for Atmospheric Science (NCAS) for the use of the sodar and radiosonde units. MISR data used in this study were produced with the Giovanni online data system, developed and maintained by the NASA GES DISC. The UK Meteorological Office, via the NCAS British Atmospheric Data Center, 2006, provided radiosonde data (http://badc.nerc.ac.uk/view/badc.nerc.ac.uk__ATOM__dataent_GLOBRADS).

[60] The FENNEC-France project is funded by the Agence Nationale de la Recherche, the Institut National des Sciences de l'Univers (INSU/CNRS) through the LEFE program, by the Centre National d'Etudes Spatiales through the TOSCA program and by Météo-France. The authors wish to thank Service des Avions Français Instrumentés pour la Recherche en Environnement and the Division Technique of INSU for preparing the research aircraft (Falcon 20/F-GBTM) and the airborne instruments in a timely manner for the FENNEC SOP.

References

Ansmann, A., A. Petzold, K. Kandler, I. Tegen, M. Wendisch, D. Muller, B. Weinzierl, T. Muller, and J. Heintzenberg (2011), Saharan Mineral Dust Experiments SAMUM-1 and SAMUM-2: What have we learned?, *Tellus Ser. B*, *63*, doi:10.1111/j.1600-0889.2011.00555.x.

Blackadar, A. K. (1955), Extension of the laws of thermodynamics to turbulent systems, *J. Meteorol*, *12*, 165–175.

Chauvin, F., R. Roehrig, and J. P. Lafore (2010), Intraseasonal variability of the Saharan heat low and its link with midlatitudes, *J. Climate*, *23*, 2544–2561.

Cuesta, J., et al. (2008), Multiplatform observations of the seasonal evolution of the Saharan atmospheric boundary layer in Tamanrasset, Algeria, in the framework of the African Monsoon Multidisciplinary Analysis field campaign conducted in 2006. *J. Geophys. Res.*, *113*. D00C07, doi:10.1029/2007JD009417.

Cuesta, J., J. H. Marsham, D. J. Parker, and C. Flamant (2009), Dynamical mechanisms controlling the vertical redistribution of dust and the thermodynamic structure of the West Saharan atmospheric boundary layer during summer, *Atmos. Sci. Lett.*, *10*, 34–42.

Cwiertny, D. M., Y. A. Young, and V.H. Grassian (2008), Chemistry and photochemistry of mineral dust aerosol. *Annu. Rev. Phys. Chem.*, *59*, 27–51.

Dee, D. P., with 35 co-authors (2011), The ERA-Interim reanalysis: Configuration and performance of the data assimilation system. *Quart. J. R. Meteorol. Soc.*, *137*, 553–597.

Dunion, J. P., and C. S. Velden (2004), The impact of the Saharan air layer on Atlantic tropical cyclone activity, *Bull. Amer. Meteorol. Soc*, *85*, 353–365.

Engelstaedter, S., I. Tegen, and R. Washington (2006), North African dust emissions and transport, *Earth-Sci. Rev.*, *79*, 73–100.

Grams, C. M., S. C. Jones, J. H. Marsham, D. J. Parker, J. M. Haywood, and V. Heuveline (2010), The Atlantic inflow to the Saharan heat low: Observations and modelling, *Quart. J. Roy. Meteorol. Soc*, *136*, 125–140.

Haustein, K., C. Pérez, J. M. Baldasano, O. Jorba, S. Basart, R. L. Miller, Z. Janjic, T. Black, S. Nickovic, M. C. Todd, and R. Washington (2012), Atmospheric dust modeling from meso to global scales with the online NMMB/BSC-Dust model: 2. Regional experiments in North Africa. *Atmos. Chem. Phys.*, *12*, 2933–2958.

Haywood, J., and O. Boucher (2000), Estimates of the direct and indirect radiative forcing due to tropospheric aerosols: A review, *Rev. Geophys.*, *38*, 513–543.

Haywood, J., P. Francis, S. Osborne, M. Glew, N. Loeb, E. Highwood, D. Tanre, G. Myhre, P. Formenti, and E. Hirst (2003), Radiative properties and direct radiative effect of Saharan dust measured by the C-130 aircraft during SHADE: 1. Solar spectrum, *J. Geophys. Res.*, *108*(D18), 8577, doi:10.1029/2002JD002687.

Haywood, J. M., R. P. Allan, I. Culverwell, T. Slingo, S. Milton, J. Edwards, and N. Clerbaux (2005), Can desert dust explain the outgoing longwave radiation anomaly over the Sahara during July 2003?, *J. Geophys. Res.*, *110*, D05105, doi:10.1029/2004JD005232.

Haywood, J. M., et al. (2008), Overview of the dust and biomass-burning experiment and African monsoon multidisciplinary analysis special observing period-0, *J. Geophys. Res.*, *113*, D00C17, doi:10.1029/2008JD010077.

Haywood, J. M., et al. (2011), Motivation, rationale and key results from the GERBILS Saharan dust measurement campaign. *Quart. J. Roy. Meteorol. Soc.*, *137*, 1106–1116, doi:10.1002/qj.797.

Hobby, M., et al. (2012), The Fennec automatic weather station (AWS) network: Monitoring the Saharan climate system, *J. Atmos. Ocean. Tech.*, doi:10.1175/JTECH-D-12-00037.1.

Holben, B. N., et al. (1998), AERONET–A federated instrument network and data archive for aerosol characterization, *Remote Sens. Environ.*, *66*, 1–16.

Jickells, T. D., et al. (2005), Global iron connections between desert dust, ocean biogeochemistry, and climate, *Science*, *308*, 67–71.

Kaufman, Y. J., I. Koren, L. A. Remer, D. Rosenfeld, and Y. Rudich (2005), The effect of smoke, dust, and pollution aerosol on shallow cloud development over the Atlantic Ocean, *Proc. Nat. Acad. Sci.*, *102*, 11,207–11,212.

Klose, M., Y. Shao, M. K. Karremann and A. H. Fink (2010), The Sahel dust zone and synoptic background. *Geophys. Res. Lett.*, *37*, L09802, doi:10.1029/2010GL042816.

Knippertz, P., and M. C. Todd (2010), The central west Saharan dust hot spot and its relation to African easterly waves and extratropical disturbances, *J. Geophys. Res.*, *115*, D12117, doi:10.1029/2009JD012819.

Knippertz, P., and M.C. Todd (2012), Mineral dust aerosols over the Sahara: Processes of emission and transport, and implications for modeling. *Rev. Geophys.*, *50*, RG1007, doi:10.1029/2011RG000362.

Lavaysse, C., C. Flamant, S. Janicot, D. J. Parker, J. P. Lafore, B. Sultan, and J. Pelon (2009), Seasonal evolution of the West African heat low: A climatological perspective, *Clim. Dyn.*, *33*, 313–330.

Lensky, I. M., and D. Rosenfeld (2008), Clouds-aerosols-precipitation satellite analysis tool (CAPSAT), *Atmos. Chem. Phys.*, *8*, 6739–6753.

Lothon, M., F. Saïd, F. Lohou, and B. Campistron, (2008), Observation of the diurnal cycle of the low troposphere of West Africa and impact on the transport of water vapour, *Mon. Wea. Rev.*, *136*, 3477–3500.

Mahowald, N. M., et al. (2010), Observed 20th century desert dust variability: impact on climate and biogeochemistry, *Atmos. Chem. Phys.*, *10*, 10,875–10,893, doi:10.5194/acp-10-10875-2010.

Marsham, J. H., D. J. Parker, C. M. Grams, C. M. Taylor, and J. M. Haywood (2008), Uplift of Saharan dust south of the intertropical discontinuity, *J. Geophys. Res.*, *113*, D21102, doi:10.1029/2008JD009844.

Marsham, J. H., P. Knippertz, N. S. Dixon, D. J. Parker, and G. M. S. Lister (2011), The importance of the representation of deep convection for modeled dust-generating winds over West Africa during summer, *Geophys. Res. Lett.*, *38*, L16803, doi:10.1029/2011GL048368.

Marsham, J., et al. (2012), Meteorology and dust in the central Sahara: Observations from Fennec superiste-1 during the June 2011 Intensive Observation Period, *J. Geophys. Res.*, *118*, 1–21, doi:10.1002/jgrd.50211, (Under review).

McConnell, C. L., E. J. Highwood, H. Coe, P. Formenti, B. Anderson, S. Osborne, S. Nava, K. Desboeufs, G. Chen, and M. A. J. Harrison (2008), Seasonal variations of the physical and optical characteristics of Saharan dust: Results from the Dust Outflow and Deposition to the Ocean (DODO) experiment, *J. Geophys. Res.*, *113*, D14S05, doi:10.1029/2007JD009606.

Messager, C., D. Parker, O. Reitebuch, A. Agusti-Panareda, C. M. Taylor, and J. Cuesta (2010), Structure and dynamics of the Saharan atmospheric boundary layer during the West African monsoon onset: Observations and analyses from the research flights of 14 and 17 July 2006, *Quart. J. Roy. Meteor. Soc.*, 107–124.

Michalakes, J., D. Duhia, D. Gill, T. Henderson, J. Klemp, and W. Wang (2005), The Weather Research and Forecast Model: Software Architecture and Performance, 2005.

Milton, S. F., G. Greed, M. E. Brooks, J. Haywood, B. Johnson, R. P. Allan, A. Slingo, and W. M. F. Grey (2008), Modeled and observed atmospheric radiation balance during the West African dry season: Role of mineral dust, biomass burning aerosol, and surface albedo, *J. Geophys. Res.*, *113*, D00C02, doi:10.1029/2007JD009741.

Parker, D. J., R. R. Burton, A. Diongue-Niang, R. J. Ellis, M. Felton, C. M. Taylor, C. D. Thorncroft, P. Bessemoulin, and A. M. Tompkins (2005), The diurnal cycle of the West African monsoon circulation, *Quart. J. Roy. Meteor. Soc.*, *131*, 2839–2860.

Perez, C., S. Nickovic, G. Pejanovic, J. M. Baldasano, and E. Ozsoy (2006), Interactive dust-radiation modeling: A step to improve weather forecasts, *J. Geophys. Res.*, *111*, D16206, doi:10.1029/2005JD006717.

Peyrille, P., and J. P. Lafore (2007), An idealized two-dimensional framework to study the West African monsoon. Part II: Large-scale advection and the diurnal cycle, *J. Atmos. Sci.*, *64*, 2783–2803.

Peyrille, P., J. P. Lafore, and J. L. Redelsperger (2007), An idealized two-dimensional framework to study the West African monsoon. Part I: Validation and key controlling factors, *J. Atmos. Sci.*, *64*, 2765–2782.

Pugh, D.T. (1987), *Tides, Surges and Mean Sea- Level*, pp. 472 John Wiley & Sons, Chichester.

Redelsperger, J. L., C. D. Thorncroft, A. Diedhiou, T. Lebel, D. J. Parker, and J. Polcher (2006), African monsoon multidisciplinary analysis – An international research project and field campaign, *Bull. Amer. Meteorol. Soc.*, *87*(12), 1739–1746.

Rodwell, M. J., and T. Jung (2008), Understanding the local and global impacts of model physics changes: An aerosol example, *Quart. J. Roy. Meteor. Soc.*, *134*, 1479–1497.

Roehrig, R., F. Couvreux, E. Poan, J. P. Lafore, O. Ndiaye, A. Diongue, F. Favot, L. Fleury, and J. L. Boichard (2012), Real-time monitoring and forecast of synoptic-to-intraseasonal variability of the 2011 West African Monsoon, paper presented at 30th Conference on Hurricanes and Tropical Meteorology, Amer. Meteor. Soc., Ponte Vedra Beach, Florida, USA.

Ryder, C. L., et al. (2013), Optical properties of Saharan dust aerosol and contribution from the coarse mode as measured during the Fennec 2011 aircraft campaign, *Atmos. Chem. Phys.*, *13*, 303–325.

Schepanski, K., I. Tegen, M. C. Todd, B. Heinold, G. Bonisch, B. Laurent, and A. Macke (2009), Meteorological processes forcing Saharan dust emission inferred from MSG-SEVIRI observations of subdaily dust source activation and numerical models, *J. Geophys. Res.*, *114*, D10201, doi:10.1029/2008JD010325.

Slingo, A., et al. (2006), Observations of the impact of a major Saharan dust storm on the atmospheric radiation balance, *Geophys. Res. Lett.*, *33*, L24817, doi:10.1029/2006GL027869.

Stensrud, D. J. (1996), Importance of low-level jets to climate: A review, *J. Climate*, *9*, 1698–1711.

Sultan, B., S. Janicot, and A. Diedhiou (2003), The West African monsoon dynamics. Part I: Documentation of intraseasonal variability, *J. Climate*, *16*, 3389–3406.

Thorncroft, C. D., et al. (2003), The JET2000 project – Aircraft observations of the African easterly jet and African easterly waves, *Bull. Amer. Meteor. Soc*, *84*, 337–351.

Todd, M. C., R. Washington, J. V. Martins, O. Dubovik, G. Lizcano, S. M'Bainayel, and S. Engelstaedter (2007), Mineral dust emission from the Bodele Depression, northern Chad, during BoDEx 2005, *J. Geophys. Res.*, *112*, D06207, doi:10.1029/2006JD007170.

Todd, M. C., R. Washington, S. Raghavan, G. Lizcano, and P. Knippertz (2008), Regional model simulations of the Bodele low-level jet of northern Chad during the Bodele Dust Experiment (BoDEx 2005), *J. Climate*, *21*, 995–1012.

Tompkins, A. M., C. Cardinali, J. J. Morcrette, and M. Rodwell (2005), Influence of aerosol climatology on forecasts of the African Easterly Jet, *Geophys. Res. Lett.*, *32*, L10801, doi:10.1029/2004GL022189.

Van de Wiel, B. J. H., A. F. Moene, G. J. Steeneveld, P. Baas, F. C. Bosveld, and A. A. M. Holtslag (2010), A conceptual view on inertial oscillations and nocturnal low-level jets, *J. Atmos. Sci.*, *67*, 2679–2689.

Washington, R., and M. C. Todd (2005), Atmospheric controls on mineral dust emission from the Bodele Depression, Chad: The role of the low level jet, *Geophys. Res. Lett.*, *32*, L17701, doi:10.1029/2005GL023597.

Washington, R., M. C. Todd, S. Engelstaedter, S. Mbainayel, and F. Mitchell (2006), Dust and the low-level circulation over the Bodele Depression, Chad: Observations from BoDEx 2005, *J. Geophys. Res.*, *111*(D3), D03201, doi:10.1029/2005JD006502.